Stochastic Optical Reconstruction Microscopy (STORM)

Jianquan Xu,[1] Hongqiang Ma,[2] and Yang Liu[3]

[1]Biomedical and Optical Imaging Laboratory, Departments of Medicine and Bioengineering, University of Pittsburgh, Pittsburgh, Pennsylvania
[2]Biomedical and Optical Imaging Laboratory, Departments of Medicine and Bioengineering, University of Pittsburgh, Pittsburgh, Pennsylvania
[3]Biomedical and Optical Imaging Laboratory, Departments of Medicine and Bioengineering, University of Pittsburgh, University of Pittsburgh Cancer Institute, Pittsburgh, Pennsylvania

Super-resolution (SR) fluorescence microscopy, a class of optical microscopy techniques at a spatial resolution below the diffraction limit, has revolutionized the way we study biology, as recognized by the Nobel Prize in Chemistry in 2014. Stochastic optical reconstruction microscopy (STORM), a widely used SR technique, is based on the principle of single molecule localization. STORM routinely achieves a spatial resolution of 20 to 30 nm, a ten-fold improvement compared to conventional optical microscopy. Among all SR techniques, STORM offers a high spatial resolution with simple optical instrumentation and standard organic fluorescent dyes, but it is also prone to image artifacts and degraded image resolution due to improper sample preparation or imaging conditions. It requires careful optimization of all three aspects—sample preparation, image acquisition, and image reconstruction—to ensure a high-quality STORM image, which will be extensively discussed in this unit. © 2017 by John Wiley & Sons, Inc.

Keywords: single molecule localization microscopy (SMLM) • stochastic optical reconstruction microscopy (STORM) • super-resolution fluorescence microscopy

How to cite this article:
Xu, J., Ma, H., & Liu, Y. (2017). Stochastic optical reconstruction microscopy (STORM). *Current Protocols in Cytometry*, *81*, 12.46.1–12.46.27. doi: 10.1002/cpcy.23

INTRODUCTION

Fluorescence microscopy is an essential tool for biologists to visualize molecular structures and their interactions. The fundamental diffraction limits the resolution of conventional microscopy to approximately half of the wavelength (~λ/2NA, where λ is wavelength and NA is the numerical aperture of the optical system). Super-resolution (SR) fluorescence microscopy, a new class of microscopy techniques that break this fundamental diffraction–limited resolution, has experienced rapid growth in the past 10 years. Various types of SR techniques have been developed, such as structured illumination microscopy (SIM; Gustafsson, 2000), stimulated emission microscopy (STED; Hell & Wichmann, 1994), (fluorescence) photo-activated localization microscopy [(f)PALM (Betzig et al., 2006; Hess, Girirajan, & Mason, 2006)], and (direct) stochastic optical reconstruction microscopy [*(d)*STORM (Heilemann et al., 2008; Rust, Bates, & Zhuang, 2006)]. These techniques either achieve sub-diffraction-limited resolution by optical manipulation of point spread function (PSF), such as in STED, or by precise localization

Current Protocols in Cytometry 12.46.1–12.46.27, April 2017
Published online April 2017 in Wiley Online Library (wileyonlinelibrary.com).
doi: 10.1002/cpcy.23

of single fluorescent emitters such as in *(d)*STORM and (f)PALM, also known as single molecule localization microscopy (SMLM).

Among state-of-the-art SR microscopy techniques, *(d)*STORM has several advantages, such as the use of standard organic fluorescent dyes and relatively simple instrumentation, as well as one of the best resolutions, down to ~20 nm. In *(d)*STORM (or SMLM), a small subset of the densely labeled fluorophores is sequentially switched "on" to achieve sparsely distributed single fluorescent emitters at each image frame, then the centers of the sparsely distributed single fluorescent emitters are determined by a localization algorithm at nanometer precision. After accumulating localized positions from a sufficiently large number of image frames (typically 5,000 to 40,000 frames), the final reconstructed image improves the resolution 10-fold. Therefore, *(d)*STORM requires synergy of all three equally important aspects: (1) proper labeling of the molecules of interest with photo-switchable fluorophores; (2) stochastic photo-activation of labeled fluorophores to achieve sparsely distributed single fluorescent emitters in the imaging field (i.e., image acquisition); and (3) precise localization of individual single fluorescent emitters at each image frame (i.e., image reconstruction). A compromise in any of these steps can lead to significant image artifacts and degradation in image resolution. Many well-written reviews have provided a detailed introduction to the general principles and labeling of photo-switchable fluorophores (Bates, Jones, & Zhuang, 2013a, 2013b; Endesfelder & Heilemann, 2015; van de Linde et al., 2011). Conventional diffraction-limited fluorescence microscopy techniques are mostly "turn-key" instruments that do not demand that users fully understand the technology itself. However, mastering *(d)*STORM requires a substantial understanding of key factors involving chemistry, optics, and image processing, which often presents a challenge to many biologists without substantial technical background (Lambert & Waters, 2016). In this unit, we do not intend to repeat the previous reviews and protocols, but focus on a comprehensive description of the protocols and interpretation of how to estimate and select all key technical factors of *(d)*STORM imaging that are critical to a high-quality and reproducible super-resolution image.

BASIC PROTOCOL 1

LABELING OF PHOTO-SWITCHABLE FLUOROPHORES

Labeling the molecular target of interest with photo-switchable fluorophores is the first critical step. Two types of photo-switchable fluorophores are used—standard organic fluorescent dyes (e.g., Alexa Fluor 647) and activator-reporter (or tandem) dye pairs (e.g., Alexa Fluor 405–Alexa Fluor 647)—and their associated imaging methods are called *direct* STORM [or *(d)*STORM; van de Linde et al., 2011] and STORM; Bates et al., 2013b), respectively. Throughout this unit, *(d)*STORM will be used if a single organic fluorescent dye is employed, STORM will be used if a dye pair is employed, and *(d)*STORM will be used if both methods are included.

Selection of proper fluorophores is the first critical step for *(d)*STORM imaging. Many organic dyes, such as cyanine, rhodamine, and oxazine dyes, have been reported to be photo-switchable under *(d)*STORM imaging conditions, but only a handful of them are good candidates for *(d)*STORM imaging. The photo-switching properties of 26 organic dyes for *(d)*STORM imaging have been extensively characterized (Dempsey, Vaughan, Chen, Bates, & Zhuang, 2011). Among all organic fluorescent dyes, Cy5 and its analog Alexa Fluor 647 are the best photo-switchable fluorophores for *(d)*STORM imaging, with excellent blinking properties, high photon counts, high signal-to-background ratio when the fluorophores are switched "on" and "off," and high duty cycles for repeated localization.

In general, two fluorescent staining methods are used—transfection of genetically engineered fluorescent protein plasmids and immunofluorescence staining. The former

applies to live cells, while the latter is commonly used in fixed cells and tissue. Here we focus on immunofluorescence staining, the most commonly used staining method for *(d)*STORM imaging. It is similar to immunostaining for conventional fluorescence microscopic imaging, but optimization in labeling density is essential to achieve high-quality and reproducible *(d)*STORM images, which is discussed in this unit.

Materials

Poly-D-lysine (PDL)
Gold nanoparticle suspension (100 nm particle size; BBI Solutions, cat. no. EM.GC100)
Alexa Fluor 405 carboxylic acid succinimidyl ester (ThermoFisher)
Alexa Fluor 647 carboxylic acid succinimidyl ester (ThermoFisher)
Cy2 and Cy3B reactive dye (GE Healthcare)
Dimethylsulfoxide (DMSO; anhydrous)
Sodium bicarbonate ($NaHCO_3$)
Secondary antibodies:
  Donkey anti-rabbit antibody (Jackson ImmunoResearch)
  Donkey anti-mouse antibody (Jackson ImmunoResearch)
Phosphate-buffered saline (PBS; Sigma-Aldrich)
Cytoskeleton buffer (see recipe)
4% (w/v) paraformaldehyde (PFA) in PBS
0.1% (v/v) Triton X-100 in PBS (permeabilization buffer)
Blocking buffer: 3% (w/v) BSA plus 0.1% (v/v) Triton X-100 in PBS
Primary antibody:
  Rabbit anti-histone H2B antibody (Abcam, cat. no. ab1790)
  Rabbit anti-alpha tubulin antibody (Abcam, cat. no. ab18251)
  Rabbit anti-H3K4me3 antibody (EMD Millipore, cat. no. 07-473)
  Mouse anti-H3K9ac antibody (Abcam, cat. no. ab12179)
Washing buffer (see recipe)

Glass bottom cell culture dishes (World Precision Instruments, cat. no. FD3510) or #1.5 coverslips
Ultrasound bath sonicator
Shaking platform
NAP-5 size-exclusion columns
Nanodrop 2000 microspectrophotometer

Preparation of glass-bottom Petri dishes or coverslips

1. Coat #1.5 coverslips or glass-bottom cell culture dish with 0.1 mg/ml poly-D-lysine (PDL) for 20 min at room temperature.
2. Wash coverslips or culture dishes once with PBS and air dry.
3. Coat with fiducial marker (optional, only needed if fiducial marker correction is used) as described below.

   Fiducial markers are used to correct sample drift. Either gold or fluorescent nanoparticles are recommended as the fiducial markers. We will take gold nanoparticles as an illustrative example.

   a. Dilute 100-nm gold nanoparticle suspension 1:50 in distilled, deionized water, sonicate in an ultrasound bath sonicator for at least 5 min, and then add the gold nanoparticle solution to PDL-coated dishes for 2 hr.
   b. Remove the solution and air dry for 10 min. Coat an additional layer of PDL to improve the cell or tissue adhesion in the steps below.

c. Check density: there should ideally be at least three fiducial markers in the field of view (FOV).

The choice between gold and fluorescent beads is made based on their susceptibility to photobleaching. If high laser power is constantly used during a long acquisition process, gold nanoparticles are preferred, as fluorescent beads can be photobleached before the completion of image acquisition. If a relatively low-power laser is used, fluorescent beads are preferred due to their high brightness.

Conjugation of photo-switchable fluorophores to secondary antibody

Fluorophore-conjugated secondary antibody used for *(d)*STORM imaging can synthesized in the laboratory. For two-color STORM imaging based on dye-pair photoswitchable fluorophores, we use the example of an Alexa Fluor 405–Alexa Fluor 647 pair and a Cy2–Alexa Fluor 647 pair of conjugated secondary antibodies; for two-color *(d)*STORM imaging, we use the example of Cy3B and Alexa Fluor 647 conjugated secondary antibodies.

4. Dissolve a 1.0 mg tube each of Alexa Fluor 405 and Alexa Fluor 647 in 100 µl of anhydrous DMSO, and divide into 50 aliquots containing 0.02 mg each. Dissolve one dye pack (1 mg) each of Cy2 or Cy3B in 20 µl DMSO and divide into 10 aliquots containing 0.1 mg each. For long-term storage, remove DMSO using a lyophilizer or evaporator and store at −20°C under dessicant.

5. Dilute the aliquot tubes of Alexa Fluor 405, Cy2, and Cy3B with 10 µl DMSO (Alexa Fluor 405: 2 µg/µl, Cy2 and Cy3B: 10 µg/µl), and dilute the aliquot tubes of Alexa Fluor 647 in 40 µl DMSO (0.5 µg/µl).

6. Prepare fresh 0.5 M $NaHCO_3$ solution.

7a. *To conjugate secondary antibodies with a single fluorescent dye for (d)STORM (using Alexa Fluor 647 and Cy3B as an example):* Thoroughly mix 40 µl donkey anti-rabbit antibody, 10 µl of 0.5 M $NaHCO_3$, and 2 µl Alexa Fluor 647 dilution from step 5 and incubate at room temperature for 30 min on a shaking platform protected from light. Similarly, mix 40 µl donkey anti-mouse antibody, 10 µl $NaHCO_3$, and 1 µl Cy3B dilution from step 5, and incubate under the same conditions.

7b. *To conjugate secondary antibodies with a dye pair:* Thoroughly mix 40 µl donkey anti-rabbit antibody, 10 µl $NaHCO_3$, 5 µl Cy2 dilution from step 5, and 1 µl Alexa Fluor 647 dilution from step 5, and incubate at room temperature for 30 min on a shaking platform protected from light. Similarly, mix 40 µl donkey anti-mouse antibody, 10 µl $NaHCO_3$, 5 µl Alexa Fluor 405 dilution from step 5, and 1 µl Alexa Fluor 647 dilution from step 5, and incubate under the same conditions.

8. During the reaction, wash the columns three times by 1000 µl PBS each time. When the reaction is complete, add 150 µl PBS to bring the reaction volume to 200 µl.

9. Add the entire reaction solution to the columns. After the last drop emerges from the bottom of the column, add 550 µl PBS to wash, then add another 300 µl PBS and collect the fluorophore-conjugated antibody in a microcentrifuge tube.

The labeled antibody is expected to elute in fraction #3 from the column.

10. Measure the absorbance of the fluorophore-conjugated secondary antibody using a Nanodrop 2000. Store the labeled antibody fraction at 4°C. For long-term storage, aliquot and store at −20°C.

11. Calculate the concentration of the dye labels using the Beer-Lambert law:

$$\text{Concentration of fluorophore} = A_{\lambda\,\max}/\varepsilon_{\lambda\,\max}$$

where $A_{\lambda max}$ is the measured absorbance maximum of the labeled fluorophore and $\epsilon_{\lambda max}$ is the extinction coefficient at the wavelength of maximum absorbance.

Extinction coefficients: Alexa Fluor 405 = 34,000 $M^{-1}cm^{-1}$ (at 401 nm), Cy2 = 150,000 $M^{-1}cm^{-1}$ (at 489 nm), Cy3B = 130,000 $M^{-1}cm^{-1}$ (at 559 nm), and Alexa Fluor 647 = 239,000 $M^{-1}cm^{-1}$ (at 650 nm).

Immunofluorescence staining (on cultured cells)

For two-color staining, two different primary or secondary antibodies are diluted at the desired concentration together in blocking buffer and incubated simultaneously.

12. Plate the cells on the coated dishes (see steps 1 to 4) at the desired density and allow them to recover overnight.

    Cytoskeleton buffer (see recipe) is recommended if microtubule or actin is imaged with STORM. Before step 2, cells are pre-extracted for 30 to 60 sec in this buffer.

    Volumes mentioned in the steps below are for cultures in a World Precision Instruments FD3510 dish.

13. Remove the medium, wash once with warm PBS, then fix with 150 µl of 4% paraformaldehyde (PFA) in PBS for 10 min.

14. Remove the fixative and wash cells twice, each time with 150 µl PBS.

15. Remove the PBS. Add 150 µl of 0.1% Triton X-100 in PBS (permeabilization buffer) to the dish and incubate for 10 min.

    If ethanol, methanol, or acetone was used to fix the cells, no permeabilization is required.

16. Wash cells three times, each time with 150 µl PBS, add 150 µl blocking buffer, and incubate for 1 hr.

    Blocking is used to prevent the secondary antibody from reacting with the unreacted aldehydes or with highly charged or very hydrophobic structures. If using polyclonal antibodies, low-affinity IgGs may bind nonspecifically to structures that are not the target of interest.

17. Dilute the primary antibody in the blocking buffer at a desired concentration (antibody dilutions: H2B antibody, 1:300; alpha tubulin antibody, 1:400; H3K4me3 antibody, 1:600; H3K9ac antibody, 1:200), add 150 µl of the diluted antibody to the cells, and incubate overnight at 4°C.

18. Wash the cells three times, each time with 150 µl washing buffer for 5 min per wash.

19. Dilute the secondary antibody conjugated with fluorescent dyes (e.g., Alexa Fluor 647) in blocking buffer at the desired concentration, add 150 µl of the antibody solution to the cells, and incubate for 2 hr at room temperature. Protect from light.

    The concentration of primary and secondary antibodies need to be optimized to achieve the best labeling density for (d)STORM imaging.

20. Aspirate and wash three times, each time with 150 µl washing buffer for 5 min per wash, then wash once with PBS.

21. Post-fix with 150 µl 4% PFA for 10 min at room temperature.

    Post-fixation is usually not needed in conventional fluorescence imaging, but it is recommended in (d)STORM imaging since long acquisition time is often needed.

22. Wash three times, each time with 150 µl PBS, and store in PBS before *(d)*STORM imaging.

IMAGE ACQUISITION

The fluorophore itself, labeled via immunofluorescence staining described above, is not photo-switchable under the imaging conditions used with conventional fluorescence microscopy. Two important factors are needed to make it photo-switchable: imaging buffer and high excitation power density (a few $kW \cdot cm^{-2}$). The imaging buffer should contain a thiol compound such as cysteamine (MEA) or 2-mercaptoethanol (β-ME), to enable photo-switching. If cyanine dyes are used, an oxygen scavenger system is also necessary to reduce the photobleaching. Similar criteria also apply to dye-pair-based STORM imaging. In this section, we describe the preparation of imaging buffer and the data acquisition steps.

Materials

Glucose oxidase from *Aspergillus niger*, type VII, lyophilized powder, ≥ 100,000 U/g solid (Sigma-Aldrich)
17 mg/ml catalase from bovine liver, lyophilized powder, ≥ 10,000 units/mg protein (Sigma-Aldrich) in buffer A
Buffer A (see recipe)
Cysteamine (MEA; Sigma-Aldrich)
0.25 N HCl
Buffer B (see recipe)
Dish with cells from Basic Protocol 1, step 22
Immersion oil for microscopy
Cyclooctatetraene (COT; Sigma-Aldrich; optional)
Fluorescence microscope

Preparation of imaging buffer

1. *GLOX:* Combine 14 mg glucose oxidase, 50 µl of 17 mg/ml catalase, and 200 µl buffer A.

   It is recommended to store the GLOX solution no longer than 1 week at 4°C.

2. *1 M MEA:* Combine 77 mg MEA plus 1.0 ml of 0.25 N HCl (pH value of the MEA solution should be in the range of 7.5 to 8.5; adjust to the range with HCl if necessary).

   This MEA stock solution can be kept at 4°C and used within 1 to 2 weeks of preparation. For long-term storage, freeze small aliquots at −20°C and keep them for several months.

3. *Imaging buffer (~1 ml):* Add 10 µl GLOX and 100 µl of 1 M MEA (or 10 µl β-ME, if β-ME buffer is to be used) to 1 ml buffer B and gently mix.

   Cyclooctatetraene (COT) is reported to significantly increase the number of photons emitted per cycle by each dye during (d)STORM imaging (Olivier, Keller, Gönczy, & Manley, 2013). Thus, 2 mM COT may optionally be added to the imaging buffer if higher photon count is required.

Data acquisition

4. Switch the PBS in the sample dish (from Basic Protocol 1, step 22) to imaging buffer, add oil to the objective, and place the dish on it.

5. Use a lower laser power (~1 mW) to identify the imaging objects and focal plane and acquire a conventional wide-field fluorescence image.

6. Increase the laser power to maximum (~2 to 10 $kW \cdot cm^{-2}$ power density) to turn "off" fluorescent molecules and trigger photo-switching.

7a. *For (d)STORM imaging:* Set the exposure time (e.g., 20 to 50 msec) and the total acquisition frame numbers (10,000 to 40,000 frames), and start the acquisition.

For (d)STORM imaging, the imaging conditions remain the same except that pulsed activation of 405 nm or 488 nm (at low power of ~1 to 100 μW) can added during data acquisition if the number of "on" molecules at each frame becomes very sparse.

7b. For *STORM imaging based on dye pairs:* One activation frame (e.g., 405 nm) and three imaging frames are typically used for each cycle, and ~10,000 cycles are often needed for each color (a total of 40,000 frames). Users can refer to the manual from N-STORM (Nikon) for detailed operation.

For example, two dye pairs are used—Alexa Fluor 405–Alexa Fluor 647 for color 1 and Cy2–Alexa Fluor 647 for color 2. Two activator lasers (405 nm and 488 nm) are pulsed on: when the 405-nm laser is pulsed on to turn on the Alexa Fluor 405–Alexa Fluor 647 channel, then the imaging laser (647 nm) is turned on for image acquisition in the color 1 channel; when the 488-nm laser is pulsed on to turn on the Cy2–Alexa Fluor 647 channel, then the 647-nm imaging laser is turned on for image acquisition in the color 2 channel.

IMAGE RECONSTRUCTION

BASIC PROTOCOL 3

Basic Protocol 2 describes how to get high-quality raw images, which ensure the subsequent reconstruction of a high-quality super-resolution image. Upon the completion of image acquisition, the final *(d)*STORM image is reconstructed by localizing single fluorescent emitters ("on" molecules) recorded at each frame. Image reconstruction software is generally provided by the commercial STORM system (e.g., N-STORM). However, there are also a large number of SMLM image reconstruction software applications made freely available with detailed documentation that have been rigorously evaluated in a recent report (Sage et al., 2015). ThunderSTORM (Ovesný, Křížek, Borkovec, Švindrych, & Hagen, 2014), a user-friendly ImageJ plugin, is one of the most widely used free software applications for *(d)*STORM image reconstruction. Alternatively, if high-speed super-resolution image reconstruction is required (e.g., online view or a very large data set with tens of millions of localization events), rapidSTORM (Wolter et al., 2012b) is also a good option. Both have detailed manuals and step-by-step guides for the image-reconstruction process. It should be noted that the selection of the proper parameters (e.g., image filtering, localization method) based on the specific raw image is critical for accurate identification of candidate single molecules and high-quality *(d)*STORM image reconstruction. Our protocol below gives a brief description of how to choose the critical parameters for *(d)*STORM image reconstruction, based on ThunderSTORM (Ovesný et al., 2014), a software application based on the free software platform ImageJ (Schneider, Rasband, & Eliceiri, 2012). Please note that the selected parameters and options described in this protocol are not the only choices. Users need to refer to their manuals for detailed guide to select the proper sets of parameters based on their specific image sets.

Materials

Raw images from Basic Protocol 2
ThunderSTORM software (*http://zitmen.github.io/thunderstorm/*)

1. Subtract the background signal from the raw image taken at each frame. In ImageJ, go to Process → Subtract Background ('Rolling ball radius' can be set to 10 pixels; see Fig. 12.46.1A-B).

2. Estimate the width of the point spread function (PSF). In ImageJ, go to the Straight Line symbol (width of 2 pixels), and draw a line across the image of a single fluorescent

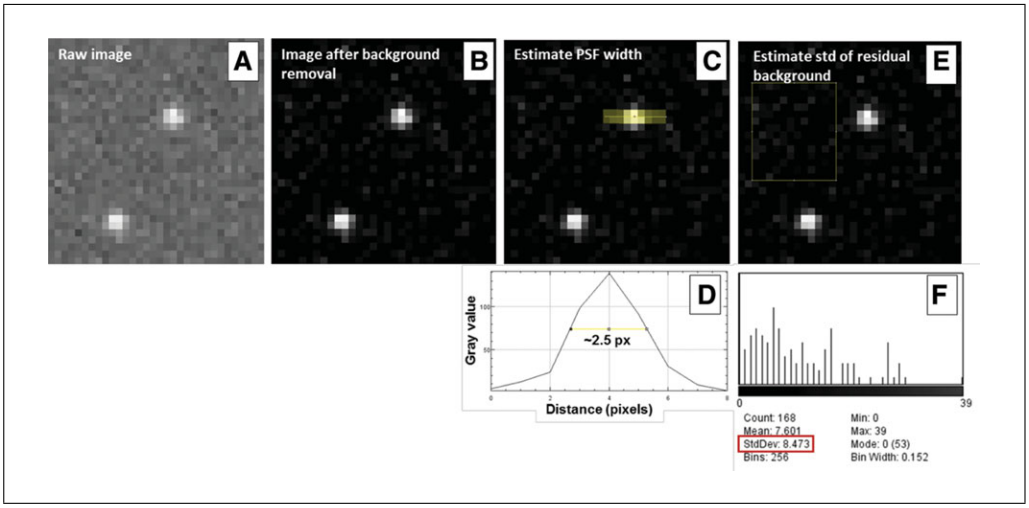

Figure 12.46.1 Illustration of how to select parameters for *(d)*STORM super-resolution image reconstruction. (**A**) Representative raw image from a single frame. (**B**) Image after background removal. (**C**) Illustration of how to estimate PSF width. A line (thickness = 2 pixels) across the yellow area in the image is plotted, shown in (**D**). The full-width at half maximum (FWHM) is shown in about 2.5 pixels. (**E**) Illustration of how to estimate standard deviation of the background. The histogram of the background in the yellow box of (C) is shown in (**F**), and standard deviation is about 8.5 pixels, shown in the red box.

emitter (see Fig. 12.46.1C). Then, go to Analyze → Plot Profile, and measure the full-width at half maximum (FWHM) of the profile.

As shown in Fig. 12.46.1D, the measured FWHM is ~2.5 pixels in our example, corresponding to the sigma (standard deviation) of the PSF of 2.5 pixels/2.35 = 1.1 pixels.

3. Set parameters in Image filtering in ThunderSTORM → Run Analysis → Image filtering (red box '1' of Fig. 12.46.2). We recommend "Difference of averaging filter," which is suitable for most *(d)*STORM raw images. The first kernel size should be slightly larger than the previously measured FWHM of PSF. In our example shown in Figure 12.46.1, we set it to 3 pixels (the measured FWHM of 2.5 pixels); the second kernel size should be at least 2 times larger than the FWHM of the PSF. In our example shown in Fig. 12.46.1, we set it to 5 pixels.

4. Set parameters in "Approximate localization molecules" in ThunderSTORM → Run Analysis (red box '2' of Fig. 12.46.2). We recommend using "Local maximum" for *(d)*STORM raw images; for "Peak intensity threshold," we recommend 3 times the standard deviation of the residual background, and in our example shown in Fig. 12.46.1, we set it to 25 (as the measured background standard deviation is ~8.5 pixels, shown in Fig. 12.46.1E-F). For "Connectivity," we recommend "8-neighbourhood" (default setting).

5. Set parameters in "Sub-pixel localization of molecules" in ThunderSTORM → Run Analysis → Sub-pixel localization of molecules (red box '3' of Fig. 12.46.2). In Method, we recommend "Gaussian PSF" or "Integrated Gaussian PSF" (their localization results do not differ much for most *(d)*STORM data), for "Fitting radius," we recommend 3 times of the PSF sigma, and in our example shown in Fig. 12.46.1, we set it to 3. For "Fitting method," we recommend "least square".

6. If the raw image consists of high-density single molecules (with overlapping fluorescent emitters), "Multi-emitter fitting analysis" box is checked.

This image-reconstruction algorithm is ~20 times slower than the single-molecule image reconstruction algorithm.

7. After all the parameters are set up, start the image reconstruction.

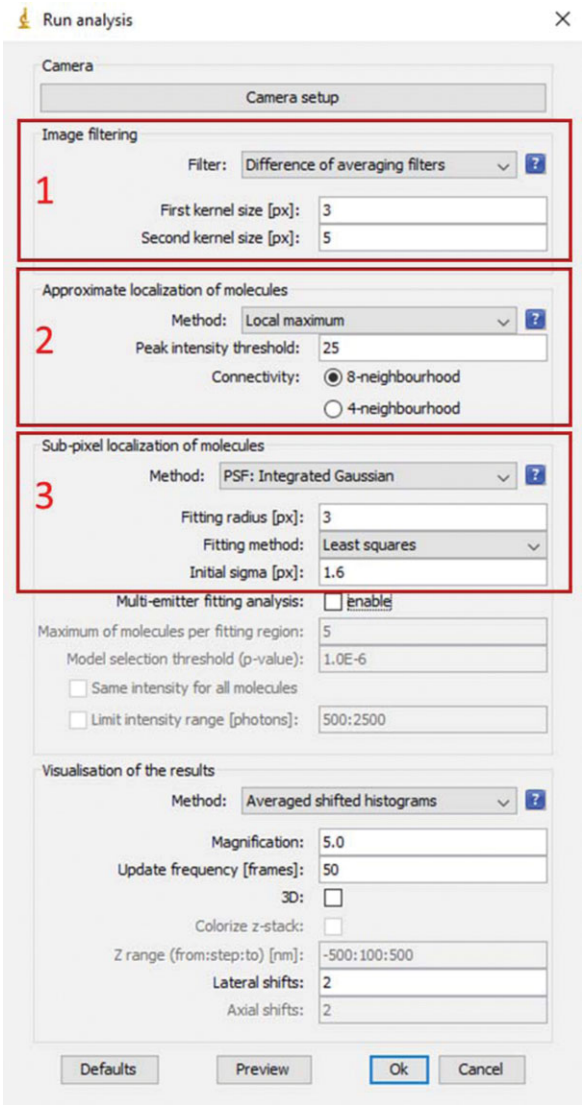

Figure 12.46.2 A snapshot of "Run Analysis" from the ThunderSTORM ImageJ plugin.

REAGENTS AND SOLUTIONS

Use deionized, distilled water in all recipes and protocol steps. For common stock solutions, see APPENDIX 2A.

Blocking buffer

Phosphate-buffered saline (PBS; Sigma-Aldrich) supplemented with:
3% (w/v) BSA
0.1% (v/v) Triton X-100
Store up to 1 month at 4°C

BRB buffer

80 mM PIPES
1 mM $MgCl_2$
1 mM EGTA
Adjust to pH 6.8 with KOH Store up to 1 year at 4°C

This solution can also be made and stored as a 5× stock.

Buffer A

0.5 ml 1 M Tris·Cl, pH 8.0 (*APPENDIX 2A*)
0.146 g NaCl
50 ml H_2O
Store up to 1 year at 4°C

Buffer B

2.5 ml 1 M Tris·Cl, pH 8.0 (*APPENDIX 2A*)
0.029 g NaCl
5 g glucose
47.5 ml H_2O
Store up to 1 year at 4°C

Cytoskeleton buffer

BRB buffer (see recipe) supplemented with:.
0.5% (v/v) Triton X-100
4 mM EGTA
Store up to 1 year at 4°C

Washing buffer

Phosphate-buffered saline (PBS; Sigma-Aldrich) supplemented with:
0.2% (w/v) BSA
0.05% (v/v) Triton X-100
Store up to 1 month at 4°C

COMMENTARY

Background Information

General information of (d)STORM imaging

The *(d)*STORM, as a single-molecule localization method in the family of SR fluorescence microscopy techniques, has a relatively unique mechanism of image formation compared to other optical methods for achieving super-resolution. It is essentially based on chemical manipulation of fluorophores to make them photo-switchable in a stochastic manner, followed by image processing to localize the individual single fluorescent emitters at nanometer precision. Unlike conventional optical microscopy where the image resolution is determined by diffraction defined by the full-width at half maximum of the point spread function (PSF), approximately $\lambda/2NA$, the *(d)*STORM image resolution is determined by multiple factors that can affect localization precision of single fluorescent emitters. Theoretically, the localization precision is expressed in terms of the standard deviation of the position measurement, $\sim s/\sqrt{N}$, where s is the standard deviation of the PSF and N is the number of collected photons. In practice, all technical factors that affect the ability to accurately localize individual fluorescent emitters can ultimately affect the image resolution. These technical factors range from instrument configuration to the properties and labeling of photo-switchable fluorophores, as well as image-reconstruction algorithms. In addition, the image resolution is also density limited. In this section, we discuss how the major technical factors affect localization precision.

STORM imaging setup and associated technical factors

A common *(d)*STORM imaging setup consists mainly of a light source for illumination, objective lens for light collection, and cameras for image detection (see Fig. 12.46.3), together with a drift correction module.

Illumination

The *(d)*STORM optical system generally requires a high-power laser to ensure that most of the fluorescent molecules are in the dark ("off") state and only a small portion of the molecules in the bright ("on") state. However, the high-power laser also increases the background signal, e.g., autofluorescence, scattered light, or non-bleached fluorescent molecules. Additional effort should be paid to decreasing the background signal. Total internal reflection fluorescence imaging (TIRF) is commonly used when the molecule of interest is within a few hundred nanometers of the surface of the coverglass. Its evanescent field

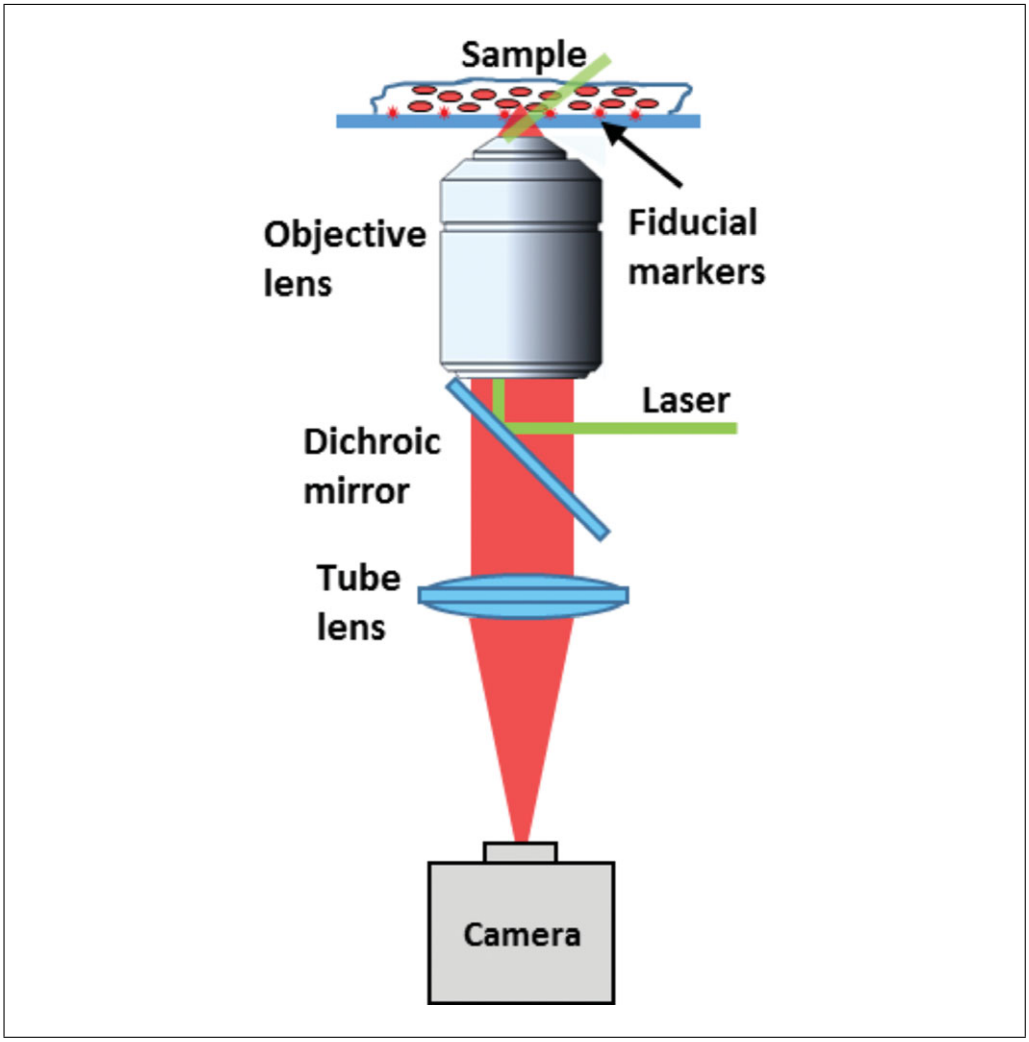

Figure 12.46.3 A simplified schematic of the *(d)*STORM instrument setup.

limits the illumination depth to be ~100 to 200 nm from the surface of the coverglass, and the background signal from those out-of-focus planes are all rejected. However, TIRF does not work if target molecules are located more than 200 nm above the coverglass surface, where high-angle inclined illumination (Tokunaga, Imamoto, & Sakata-Sogawa, 2008) or light-sheet illumination (Galland et al., 2015; Gebhardt et al., 2013) is needed. High-angle inclined illumination is easier to implement, and hence is widely used (such as in the commercial STORM system); a thinner depth of illumination provides a better reduction of the background, but results in a smaller imaging FOV that limits the throughput. In comparison, light-sheet illumination requires an additional illumination path in the optical system, and its orthogonal arrangement between illumination and collection objectives also limits the NA of the objectives and complicates the sample holder. Hence, it is not commonly used in STORM systems, but its ability to illuminate a large FOV with a relatively thin section (several microns) makes it potentially attractive for high-throughput imaging. It should be noted that if the sample is very thin (a few microns such as COS-7 cells), the illumination methods do not matter much and even conventional epi-illumination can be used (Douglass, Sieben, Archetti, Lambert, & Manley, 2016).

Objective lens

The *(d)*STORM usually uses an objective lens with high numerical aperture (NA) to collect the fluorescence signal. One advantage is that the localization precision of single molecules is proportional to the diffraction-limited resolution, which is inversely proportional to the NA of the objective, and a higher NA leads to better localization precision. The other advantage is that an objective lens with higher NA can collect more photons to increase the total photon number for each single fluorescent emitter, which also improves the

localization precision. To be more specific, for example, the commonly used objective lens for *(d)*STORM has an NA of 1.49, corresponding to a collection half angle of ~80° and a collection efficiency of ~42%; if the objective lens with NA of 1.3 is used, the collection half angle is ~59° and the collection efficiency reduces to ~25%. So, the final localization precision with an objective of NA = 1.49 is 50% better than that with an objective of NA = 1.3. Hence, in practice, we usually select an objective lens with a NA higher than 1.4.

In addition, if TIRF illumination is used, the NA of the objective lens has to be higher than 1.4 to create the critical angle. When using a high-NA objective lens, the user should note that, due to the refraction index mismatch of the imaging buffer (~1.33) and immersion oil (~1.515), the spherical aberration becomes significant at a large imaging depth (>10 μm), where adaptive optics or water-immersion objective lens can be introduced to reduce the aberration.

Camera

Super-resolution localization microscopy usually uses high-end scientific cameras (EMCCD or sCMOS) with high quantum efficiency (QE) and low noise. Lots of factors can influence the performance of a camera, such as dark current noise, read noise, fixed pattern noise, excess noise, and QE. The scientific cameras usually employ deep cooling to make the thermally induced "dark current" negligible (< 0.1 electron per frame) and a back-illuminated sensor manufacturing technique to increase the QE of the sensor up to 95%, thus preserving almost all the photons in the image recording process.

The EMCCD and sCMOS cameras adopt different technical routes to minimize noise. EMCCD uses the same gain register and A/D converter for all the pixels, so its fixed pattern noise from different signal response can be neglected, but its relatively slow read speed limits the speed of image acquisition. In addition, EMCCD uses an on-chip electron-multiplication process, which can enhance the signal and suppress the read noise to be less than 1 electron. But the electron-multiplication process is a double-edged sword—it suppresses the read noise, but introduces excess noise on each pixel and decreases the localization precision by a factor of $\sqrt{2}$ (Mortensen, Churchman, Spudich, & Flyvbjerg, 2010; Quan, Zeng, & Huang, 2010b). In comparison, sCMOS assigns a specific gain register to each pixel and A/D converter to each column, and hence the read speed is much faster than EMCCD, but its high fixed pattern noise needs additional correction in the post-processing (Huang et al., 2013). The sCMOS does not have specific electron multiplication registers, so the read noise of sCMOS cameras is above 1 electron, but without adding excess noise.

Should the user select an EMCCD or sCMOS camera? The CMOS manufacturing technique has achieved significant advances in recent years, and sCMOS is becoming an excellent alternative to EMCCD cameras. For most *(d)*STORM imaging applications, the performance of sCMOS cameras in terms of localization precision is even better than that of EMCCD. In addition, sCMOS cameras significantly improve the throughput by offering a larger FOV. In comparison, EMCCD is not only more expensive, but also has a smaller FOV, and its SNR advantage is only useful in very weak light level (< 3 photons per pixel), which is not needed under most *(d)*STORM imaging conditions. Figure 12.46.4 shows the estimated SNR for EMCCD, sCMOS (including both the first and second generation sCMOS sensors), and regular cooled interline CCD cameras; sCMOS clearly shows a better SNR when the number of photons per pixel is larger than 20. Although EMCCD is traditionally used for single-molecule imaging and *(d)*STORM, sCMOS has gradually replaced EMCCD as the preferred detector for single molecule localization microscopy. For example, the second-generation N-STORM system (N-STORM 4.0) uses sCMOS in place of the EMCCD used in their first-generation system.

Drift correction

Motion blur due to sample drift is one of the major causes of image distortion in super-resolution imaging; it results from various sources such as mechanical vibration and thermal expansion. Therefore, online drift correction is generally used for image acquisition that requires a relatively long time (several minutes), especially in *(d)*STORM. Various methods have been developed to compensate the sample drift during data acquisition. The axial depth of focus is usually less than 1 μm, so the axial drift needs to be corrected online if the axial stability of the microscopy system is not sufficient. In comparison, the lateral FOV is usually much larger (tens of microns), and thus the lateral drift can be corrected in the post-processing step.

Commercial SR microscopy systems use the infrared light that is reflected at the interface between the coverglass and the

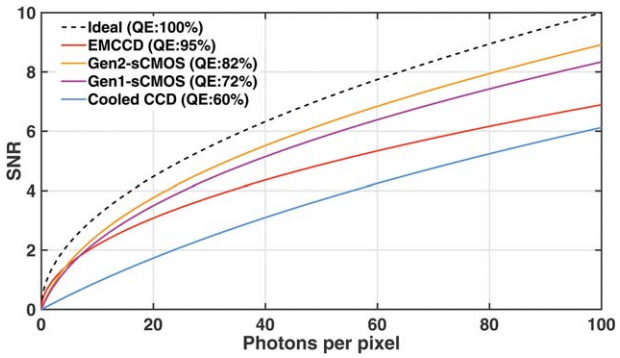

Figure 12.46.4 Comparison of SNR performance for the commonly used cameras at different signal levels. Here, only quantum efficiency (QE) and read noise are considered because the dark current noise can be ignored under deep cooling. The SNR is defined as: $SNR = Signal \cdot QE / \sqrt{Signal \cdot QE + ExcessNoise \cdot Signal \cdot QE + ReadNoise^2}$ $\begin{cases} ExcessNoise = 1, EMCCD \\ ExcessNoise = 0, other\ cameras \end{cases}$.

imaging medium due to their refractive index mismatch to monitor the drift in the axial direction (Bates et al., 2013b), and use image cross-correlation methods to correct for the lateral drift during the image-reconstruction step (Mlodzianoski et al., 2011; Wang et al., 2014). This combination can handle the drift correction in most situations, but the reflection-based axial drift correction method does not work well when the refractive indices between the coverglass and the medium are close; also, the image correlation–based lateral drift correction method depends heavily on the image content and sample structure, and it does not work well when the imaged target is dynamic in the imaging process or when there are low numbers of imaged molecules. In this context, fiduciary markers (gold or fluorescent nanoparticles attached to the surface of the coverglass) are introduced (Lee et al., 2012; Pertsinidis, Zhang, & Chu, 2010). By tracking the position of the markers on the coverglass, the precise drift in three dimensions is monitored online. When the imaging plane is distant from the focal plane where the fiduciary markers are located (e.g., a few microns above the coverglass surface), an additional "jump" process between the focal planes of the imaging objects and the fiduciary markers (e.g., every few seconds assuming no axial drift in a short time period) is needed in the image acquisition process (York, Ghitani, Vaziri, Davidson, & Shroff, 2011). Figure 12.46.5 shows an example of *(d)*STORM image of nucleosomes of the cell nucleus (histone protein H2B is labeled by Alexa Fluor 647) before and after drift correction, where the focal plane of the imaging object is about 2 to 3 µm above the surface of the coverslip where the fiduciary markers are located. This comparison highlights the importance of drift correction in *(d)*STORM imaging.

Image reconstruction

The high-quality raw image is the key prerequisite for the subsequent reconstruction of a high-quality *(d)*STORM image. Single-molecule based super-resolution image reconstruction generally comprises three steps.

Background estimation

Background is common in *(d)*STORM imaging, are located more than 3 µm above the coverslip surface. Various sources can contribute to the background signals, such as autofluorescence, scattering, and non-bleached fluorescent molecules close to and distant from the focal plane. High background signals not only degrade the localization precision, but also increase fake localization events, leading to reconstruction artifacts. Figure 12.46.6 shows the effect of background on localization precision, where the presence of a high background (B, D) leads to a reduced localization precision compared to that in the case of a low background (A, C). If the background is non-uniform, the localization position can be shifted toward the region with brighter background, resulting in severe localization bias, as shown in Fig. 12.46.7, where the localized position is shifted from the true position. Therefore, precise background estimation is highly important in these situations to remove the effects that can negatively affect the localization precision. The background can be classified into two types: (A) background with a small change between subsequent frames, which

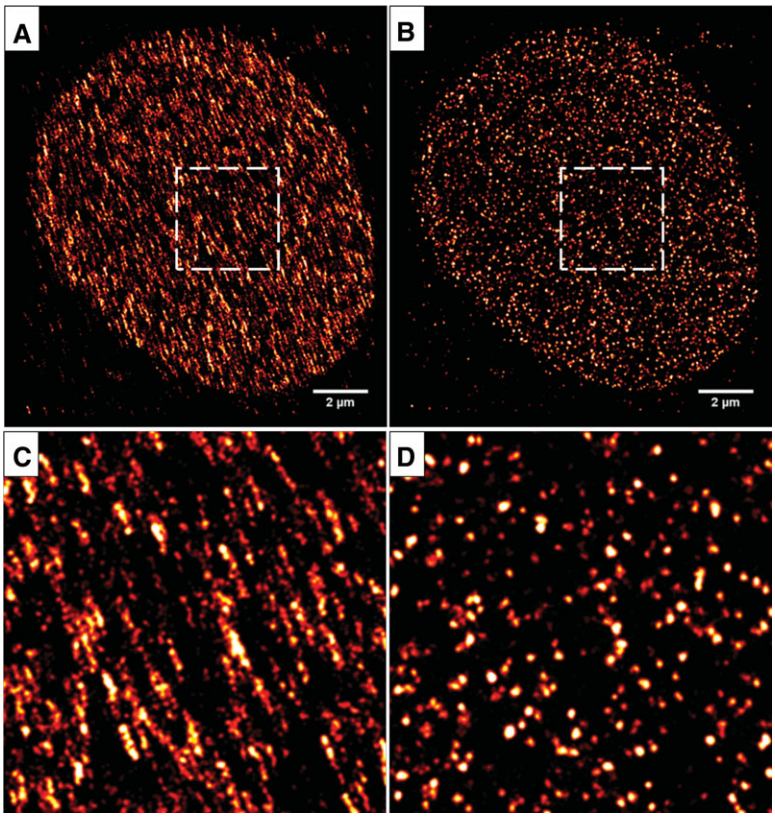

Figure 12.46.5 Super-resolution *(d)*STORM images of nucleosomes (H2B immunostained with Alexa Fluor 647) in the cell nucleus (**A**) before and (**B**) after the drift correction. The focal plane of the imaging object is ~2 to 3 μm above the surface of the coverslip. (**C**-**D**) The zoomed-in region of the white box in in A and B.

mainly consists of auto-fluorescence and non-bleached out-of-focus fluorescent molecules; and (B) background that changes every imaging frame, which is mainly from non-bleached fluorescent molecules near the focal plane. For Type (A) background, temporal filters (e.g., temporal median filter; Hoogendoorn et al., 2014) can be used for background estimation; for Type (B) background, low-pass filters (e.g., wavelet transform) can be used for background estimation.

Identification of candidate molecules

Identifying the single fluorescent emitters (bright spots) from the raw image at each frame is much simpler if the background is well estimated. To highlight the candidate molecules, different filters can be used, such as a Gaussian smoothing filter, difference of Gaussian filter, difference of mean filter, or wavelet de-noising filter. Bandpass filters (difference of Gaussian, difference of mean, and wavelet de-noising filters) can efficiently highlight the fluorescent emitters and, more importantly, are robust to the influence of residual background if the background is not well estimated. Then, the pixel with local maxima is recognized as the center of the candidate molecules, and the corresponding region of interest (ROI) is delivered to the next step for localization. This step also implements another important task—rejecting overlapped molecules—because most single-molecule localization algorithms can only precisely localize well-separated individual molecules without overlap. So, candidate molecules with distance less than the diameter of the PSF can be rejected in this step, saving computation time.

Single-molecule localization

The most rigorous method to localize single molecules from the diffraction-limited image is to fit the raw data with a PSF model and vary the parameters to minimize the difference between the raw data and PSF model. In practice, a Gaussian function is typically used to approximate the PSF model, and shot noise is used as the noise model. The fitting process is usually implemented by mathematical optimization routines. The two most

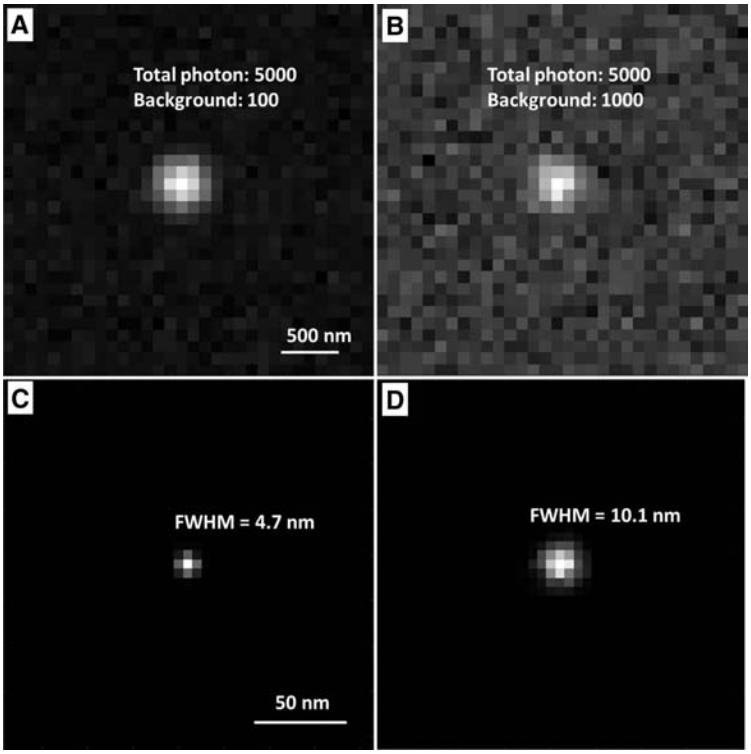

Figure 12.46.6 Effect of different background levels on the localization accuracy. (**A**, **C**) The raw image and localized (**B**, **D**) super-resolution image of a single fluorescent emitter at a low background level of 1000 photons per pixel and a high background level of 1000 photons per pixel, respectively, with total photon number for a single fluorescent emitter set to 5000 to mimic the emission properties of Alexa Fluor 647. The final localization precision, measured by the standard deviation of localized positions, is reduced by a factor of >2 at a high background level compared to a low background level. Total photon number of a single fluorescent emitter, 5000. Pixel size of the raw image: 100 nm; pixel size of the super-resolution image: 5 nm.

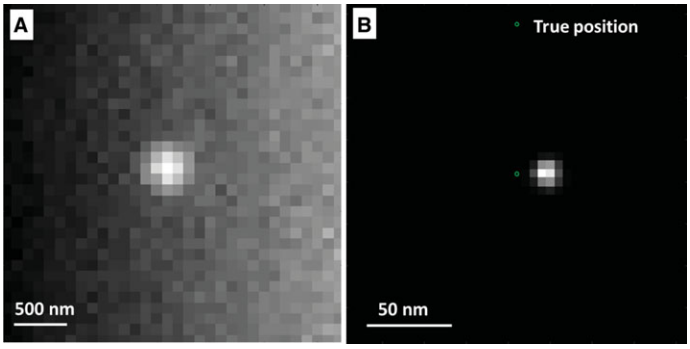

Figure 12.46.7 Effect of non-uniform background on the localization accuracy. A non-uniform background leads to significant localization bias. (**A**) From left to right, the background is simulated as 100 to 500 photons per pixel. (**B**) The localized position carries a bias of over 15 nm at a localization precision of $\sim$10 nm. Total photon number of a single fluorescent emitter: 5000. Pixel size of the raw image: 100 nm. Pixel size of the super-resolution image: 5 nm.

commonly used methods for the optimization routine are least-square estimation (LS) and maximum likelihood estimation (MLE).

Maximum likelihood estimation (MLE) is thought to be the most precise method that can reach the theoretical limit (Mortensen et al., 2010). MLE requires an accurate PSF model and noise model, as well as accurate camera information, and by varying the model parameters, it searches the parameters to

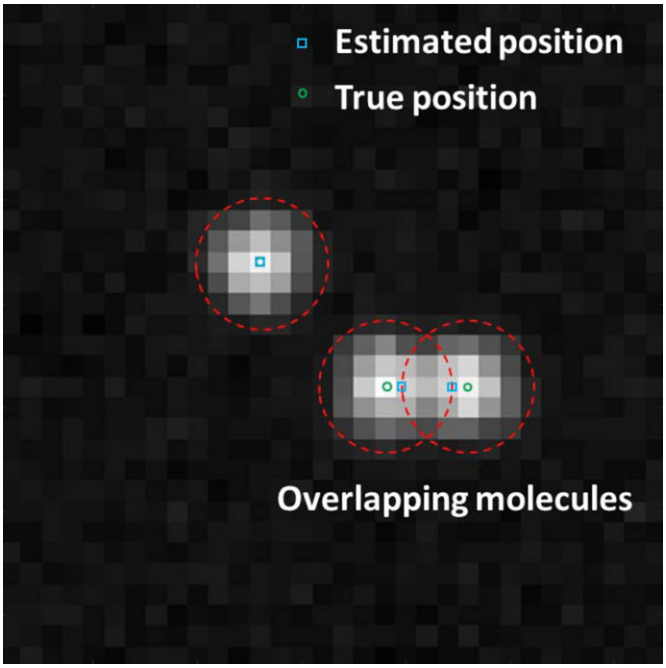

Figure 12.46.8 Effect of overlapping molecules on the localization accuracy. (**A**) Simulated raw image with overlapping molecules, defined as molecules with a distance between them less than the diameter of the PSF. (**B**) The localized positions exhibit a significant bias of over 10 nm, compared to the ground truth. Total photon number of a single fluorescent emitter: 5000. Pixel size of the raw image: 100 nm.

maximize the joint likelihood (defined as the product of the likelihood of signals on each pixel) between the model and the data. In practice, a threshold is often set to stop the iteration if the parameters are precise enough. As this process usually takes tens of iterations, its computation speed is usually slow. Therefore, multi-core CPUs or GPUs are usually used to accelerate the computation speed of MLE (Quan et al., 2010a; Smith, Joseph, Rieger, & Lidke, 2010; Wolter et al., 2012a).

However, it is not always possible to get the exact information about the PSF model, noise model, and camera, in which case least squares estimation (LS) is a better fitting tool. LS fitting requires no detailed knowledge of the camera noise, and searches the parameters that can minimize the difference between the model and the raw data. Compared to MLE, LS requires less detailed information on the noise model and camera, and is more robust to PSF distortion caused by aberration or scattering (Ovesný et al., 2014; Wolter et al., 2012a).

Generally speaking, localization fitting methods (especially MLE) work best when accurate noise and PSF models are available. However, when computational simplicity (e.g., implemented on chip) or computing speed (online analysis) is crucial, a single-iteration algorithm is often preferable. Some single-iteration algorithms such as radial symmetry (Ma, Long, Zeng, & Huang, 2012; Parthasarathy, 2012) and gradient fitting (Ma et al., 2015) have similar localization precision as the iterative fitting–based algorithms, but can run two orders of magnitude faster and hence can also be used to identify the starting values for an iterative fitting routine.

Single molecule versus high-density molecule localization

Conventional *(d)*STORM imaging requires the fluorophores to be sparsely activated without overlap. Figure 12.46.8 shows the effect of overlapping molecules on localization accuracy. In the image reconstruction process using single molecule localization algorithms, the overlapping molecules are rejected for better localization precision. To reconstruct a super-resolution image with sufficient localization density requires accumulating tens of thousands of imaging frames, which takes 10 to 15 min, resulting in a low throughput. High-density molecule localization is proposed as a strategy to improve the throughput and imaging speed by increasing the number of activated single molecules at each frame with

a reduced number of imaging frames. In addition, when the structure of the imaging object itself is highly condensed, as with chromatin, overlapping molecules are always present due to the highly compact structure.

Algorithms to localize overlapping molecules can be classified into two types: multi-emitter fitting–based algorithms (Holden, Uphoff, & Kapanidis, 2011; Huang, Schwartz, Byars, & Lidke, 2011; Quan et al., 2011) and deconvolution-based algorithms (Mukamel, Babcock, & Zhuang, 2012; Zhu, Zhang, Elnatan, & Huang, 2012). The first category fits a multiple-emitter Gaussian PSF model to the raw data, which is a straightforward extension of the single-molecule fitting. The model is a sum of PSFs at different positions, in which the number of single emitters is one of the parameters optimized to minimize the mismatch between the raw data and the model, using similar mathematical optimization routines—MLE and LS. Similar to the single-molecule fitting algorithm, MLE performs better if the PSF model, noise model and camera information are known. An important parameter for multi-emitter fitting is the estimated molecule number, which can significantly affect the final localization precision.

Deconvolution-based algorithms estimate a local density of emitters. Density is estimated on a grid that is finer than the raw image (e.g., 1/8 pixel), and the density should be 0 everywhere except at the position of an emitter. In SMLM, this task has been accomplished by Richardson-Lucy (RL) deconvolution (Mukamel et al., 2012) and compressed sensing (CS; Zhu et al., 2012). Because the high-density localization algorithms run much slower than single-emitter localization algorithms, a GPU has been introduced to accelerate the computation speed. But even with the GPU, it is still impossible to carry out ultrahigh-speed data analysis such as online image reconstruction on large data sets (e.g., tens of millions of localized molecules). The single-iteration algorithm can potentially improve the computation speed, but no closed-form mathematical solution is currently available due to the complexity of the overlapping emitter model. Note that the precision of high-density localization (even with state-of-the-art algorithms) is often compromised compared to those of sparsely distributed single-molecule localization, despite higher throughput. Therefore, if the user wants the highest resolution possible, it is important to ensure sparsely distributed single fluorescent emitters at each image frame.

Measure of (d)STORM image resolution

The resolution of the *(d)*STORM image is affected by a multitude of factors such as localization precision, Nyquist resolution, labeling density, and the underlying spatial structure of the imaging object. To objectively measure the image resolution of SMLM or *(d)*STORM, Fourier ring correlation (FRC; Nieuwenhuizen et al., 2013) is introduced, which can be computed directly from the experimental data alone without any *a priori* information. FRC resolution makes it possible to compare the resolution of images taken with different nanoscopy methods, to optimize and rank different emitter localization and labeling strategies, and to define a stopping criterion for data acquisition. However, it should be noted that FRC resolution is also affected by the sample structure and density of localizations; hence, the comparison should be based on similar sample structure and labeling density.

Multicolor (d)STORM imaging

Conventional multicolor imaging is realized by labeling the molecules of interest with dyes at different emission wavelengths. The same approach is also applicable to multicolor *(d)*STORM imaging, in which the only difference is the use of photo-switchable fluorophores.

For multicolor *(d)*STORM imaging, the selection of appropriate photo-switchable fluorophores is critical. On the one hand, since the organic dyes usually have wide absorption and emission spectra, it is important to choose dyes with well-separated spectra to avoid or maximally limit the cross-talk. On the other hand, the chosen fluorophores must show good photo-switching ability, which can significantly affect the quality of the super-resolution image. Generally, the photo-switching fluorophore that can be used in *(d)*STORM imaging should meet the following requirements: (1) high photon counts per switching cycle; (2) low fraction of time the dye spends in its "on" state (on-off duty cycle); and (3) high survival fraction and number of switching cycles. High photon count ensures a high localization precision, and low duty cycle ensures that a small fraction of molecules are in the "on" state to avoid overlapping molecules. As the image resolution of *(d)*STORM is density limited, the third factor leads to multiple repeated localizations per molecule with a higher precision.

More than 26 organic dyes have been evaluated for *(d)*STORM imaging. Although most organic fluorescent dyes exhibit some

photo-switchable properties under the same *(d)*STORM imaging conditions, most of them do not meet the above criteria as candidates for *(d)*STORM imaging. Among them, ATTO 488, Alexa Fluor 568 (substitutable by Cy3B), Alexa Fluor 647 (substitutable by Cy5), and Alexa Fluor 750 are recommended for multicolor *(d)*STORM. Because of their exceptional photo-switching properties, either Alexa Fluor 647 or Cy5 is recommended as the most ideal fluorescent dye if only single-color *(d)*STORM imaging is needed.

Alternatively, a "dye pair" scheme can be used (Bates, Huang, Dempsey, & Zhuang, 2007), in which a cyanine dye (Alexa Fluor 647/Cy5/Cy7) and a shorter-wavelength fluorophore (Alexa Fluor 405/Cy2/Cy3) are paired in close proximity by conjugating to an antibody or double-stranded DNA, referred to as a "reporter" and "activator," respectively. These reporter dyes display robust photo-switching behavior upon re-activating them with the "activator" wavelength. Multicolor STORM imaging can be implemented by using an identical reporter dye paired with different activator dyes (e.g., Cy2-Cy5 and Cy3-Cy5) or using different reporter dyes paired with same activator dye (e.g., Cy3-Cy5 and Cy3-Cy7).

Critical Parameters and Troubleshooting

Choice of fixatives

The main objective of fixation is to preserve cells and tissue in as close to their natural state as possible, thereby preventing autolysis or putrefaction. Crosslinking and protein precipitation are the two general approaches for cell fixation. Crosslinking fixatives such as PFA fix cells or tissue by forming covalent chemical bonds between proteins, while precipitating fixatives such as methanol, ethanol, and acetone act by reducing the solubility of protein molecules. Since the membrane is permeabilized by precipitating fixatives, there is no need to permeabilize with Triton after fixation, as with crosslinking fixatives.

All the fixatives have their advantages and disadvantages. Fixative should be carefully selected, and the fixation protocol should also be optimized depending on the target molecules of interest. For example, cold methanol shows good results in microtubule fixation, alcohol fixative performs well on nucleic acids, and formaldehyde is commonly used in tissue fixation and preserves most antigens. Overall, the selection of appropriate fixative should meet the following three criteria: (1) best preserving the original structure and morphology of cells or tissue; (2) best preserving the activity of antigens; and (3) avoiding the use of fixatives that can cause autofluorescence. For example, aldehyde fixatives react with amines and proteins to generate fluorescent products, and glutaraldehyde is worse in this respect than formaldehyde. If glutaraldehyde has to be used for fixation, the sample can be reduced with freshly prepared 0.1% $NaBH_4$ solution to bleach the autofluorescence. Therefore, the type of fixative, fixation time, temperature, and pH values can all affect the experimental results.

Immunostaining

The most important parameter in the immunofluorescence staining step for *(d)*STORM imaging is to optimize the labeling density. As the resolution of the *(d)*STORM image depends on labeling density, a lower labeling density significantly compromises the image resolution and results in serious image artifacts. Figure 12.46.9 shows an example of reconstructed *(d)*STORM images of H2B in cases of low labeling density and high labeling density via immunofluorescence staining with Alexa Fluor 647. Although the conventional wide-field images appear similar (see insets in Fig. 12.46.9A,C), their corresponding *(d)*STORM images (Figs. 12.46.9A,C) exhibit distinct structures. The reconstructed *(d)*STORM image in the case of a low labeling density (Fig. 12.46.9E) exhibits more diffuse structural features without distinct cluster-like nucleosomes, while the heterogeneous and discrete nucleosome clusters (Ricci, Manzo, García-Parajo, Lakadamyali, & Cosma, 2015) become distinctly clear in the case of a high labeling density (Fig. 12.46.9G). It should be noted that Gaussian rendering (via a Gaussian blur filter) is often used in the *(d)*STORM image rendering step to minimize the effect of image pixilation and improve the visualization (see Fig. 12.46.9B, D, F, H). Such image processing should not dramatically change the structure presented in the image (see Fig. 12.46.9C, G versus Fig. 12.46.9D, H). However, for the case of low labeling density, the smoothed image can amplify the image artifact (see Figs. 12.46.9A, E versus Fig. 12.46.9D, F).

To ensure sufficient labeling density, we suggest using a higher antibody concentration than the one recommended by the suppliers, which is often tested for conventional immunofluorescence staining. We also recommend a blocking step to minimize

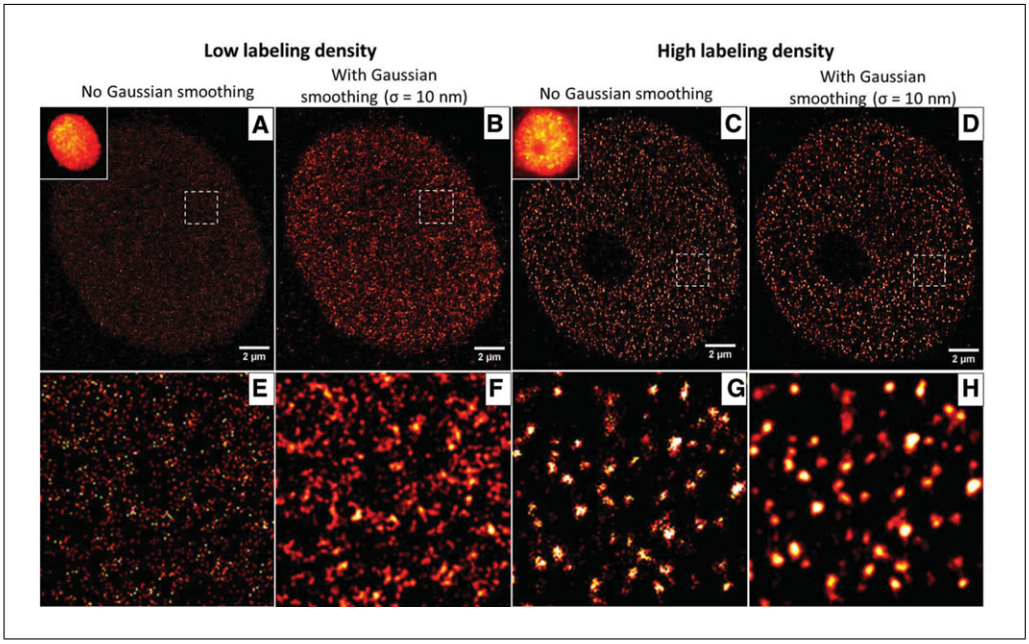

Figure 12.46.9 Reconstructed *(d)*STORM images of H2B. (**A**-**B**, **E**-**F**) Low labeling density; (**C**-**D**, **G**-**H**) high labeling density. (A-B) The *(d)*STORM images of H2B in the case of low labeling density before and after applying a Gaussian smoothing filter ($\sigma = 10$ nm). (C-D): The reconstructed *(d)*STORM images of H2B in the case of high labeling density before and after applying the same Gaussian smoothing filter as (B). The figure insets of (A,C) are the corresponding wide-field image of H2B. (E-H): The zoomed-in region of the white boxes shown in (A-D).

nonspecific binding. Additionally, we recommend incubating the primary antibody overnight at 4°C (rather than a few hours used by immunofluorescence staining for conventional fluorescence imaging) and incubating the secondary antibody at least 1 hr at the room temperature.

The fluorophore-conjugated secondary antibodies are often commercially available, and they are routinely used for conventional imaging. However, since they are typically not well validated for *(d)*STORM imaging, in our experience, the performance of commercial antibodies from different companies or with differ lot numbers is variable. Many commercially available fluorophore-conjugated antibodies do not provide sufficient labeling density, leading to low localization number in the reconstructed *(d)*STORM image, even if a decent wide-field image can be obtained. Further, the antibody-to-dye ratio is often unclear or variable from lot to lot. Therefore, we recommend conjugating the fluorophores with secondary antibody in the laboratory for *(d)*STORM imaging, rather than using commercially available fluorophore-conjugated secondary antibodies. The secondary antibodies can react with dyes with an NHS ester group under alkalescent condition (pH ~8.5), which can be accomplished in most research laboratories according to the manufacturer's protocol or the protocol outlined in this unit.

In addition, antibody validation, which is an important process for any antibody-based assay, is even more important for *(d)*STORM imaging. Some commercially available antibodies do not meet the criterion of high labeling density for *(d)*STORM imaging due to their poor labeling efficiency, even when they are sufficient for conventional microscopy. Therefore, the antibody first needs to be validated to ensure sufficient labeling density and localization number for the structure of interest. Although there is no well-defined localization number needed for the imaging object, too low a localization number (1 to 2) from a structure of interest requires extra caution to ensure that the *(d)*STORM image is the true representation of the imaging object. Therefore, for primary antibodies, it is always recommended to choose those with high specificity and sensitivity [e.g., ChIP Grade, Knockout (KO) validated antibodies]. For secondary antibodies, we recommend using those with fluorophore conjugation performed in the laboratory as described in this unit.

Imaging buffer

The photo-switching properties of the fluorophore highly depend on the presence of imaging buffer. The ideal photo-switching

properties for *(d)*STORM imaging are that the majority of the fluorophores stay in the dark ("off") state for a long period of time (several minutes) to prevent high background, while only a small portion of the fluorophores stay in the "on" state for a short time period of tens of milliseconds with a high photon count. Besides the properties of the fluorophore itself, two factors in the imaging buffer significantly affect the photoswitching properties of the fluorophore—thiol concentration and oxygen scavenger system. Upon photoexcitation, the fluorophore reacts with thiol in solution and forms intermediate states that turn dark ("off" state). The dark state has a long lifetime and returns to the "on" state spontaneously (Dempsey et al., 2009; van de Linde et al., 2011). Oxygen removal reduces the effect of photobleaching (Dempsey et al., 2009) and increases the lifetime of the intermediate states (van de Linde et al., 2011), especially for cyanine dyes (e.g., Alexa Fluor 647 or Cy5). Therefore, both thiol concentration and oxygen scavenger are required for proper photoswitching properties.

There are two types of thiols commonly used in *(d)*STORM imaging, 2-mercaptoethanol (β-ME) and MEA. In some cases, the switching behavior of the dyes is rather sensitive to the type of thiol, as well as its concentration. For example, 2-mercaptoethanol-containing buffer provides a higher photon count per switching cycle for Alexa Fluor 647/Cy5, and MEA has a longer duty cycle, which is good for densely labeled samples. A moderate to low concentration of MEA enhances photo-switching rates, but high concentrations of MEA diminish either the number of switching cycles or the number of photons per switching cycle (Bates et al., 2013b). Generally, if the photoswitching rate is too low, decrease the MEA concentration or pH value, and vice versa.

On the other hand, an oxygen scavenging system is usually required in *(d)*STORM imaging to improve photo-switching of the fluorophore. The most commonly used oxygen scavenging system consists of a combination of glucose, glucose oxidase, and catalase. However, this system results in a time-dependent acidification of the buffer caused by the accumulation of the byproduct—gluconic acid. An alternative oxygen scavenging system is a combination of protocatechuic acid and protocatechuic dioxygenase (PCA/PCD), which provide stable pH over several hours, but it is more expensive compared to the glucose-based system.

During the long imaging process, when the molecular O_2 reacts with the oxygen scavenging system in the imaging buffer, resulting in a decrease in the pH value, the photo-switching properties of the fluorophore can be significantly compromised. Therefore, we recommend using fresh imaging buffer and replacing the buffer at the appropriate time. The time interval for replacing the buffer depends on the volume of the buffer added to the sample. For the dishes use in this protocol (World Precision Instruments, cat. no. FD3510) which contain ~200 µl buffer, we recommend using the imaging buffer for no more than 1 hr. If the sample is well sealed with minimal influx of atmospheric oxygen, the imaging buffer can last a few hours (Nahidiazar Agronskaia, Broertjes, van den Broek, & Jalink, 2016).

Image acquisition

In the image-acquisition step, two parameters are important—exposure time and the number of image frames to be collected. Theoretically, the exposure time should be adjusted to be equal to the "on" time of the fluorophore, to maximize the collected photons from each switching cycle in a single image frame. A higher power of excitation laser can also increase the blinking rate of the fluorophore, thus improving the data-acquisition speed. However, if the laser power is too high, it can cause significant thermal damage to the sample and the optics during a long period of data acquisition. Users should confirm minimal damage if a high laser power density (e.g., >5 kW/cm^2) is used.

Selecting a sufficient number of imaging frames is important to faithfully reconstruct the super-resolution image in *(d)*STORM, and too few frame numbers can lead to significant image artifacts. Figures 12.46.10 and 12.46.11 show examples of reconstructed *(d)*STORM images based on different numbers of frames. The number of frames highly depends on whether the structures of interest can be densely labeled or not. For example, the ultrastructure of the densely labeled microtubules can be seen after accumulating ~5,000 frames, while the structure of nucleosomes (labeled by histone protein H2B) requires the accumulation of ~20,000 frames to present the unambiguous nucleosome clusters. Such difference often depends on the structure itself and antibody efficiency if the labeling density is already optimized. A high localization number increases the image contrast and visualization, which is often preferred. It should be noted that additional

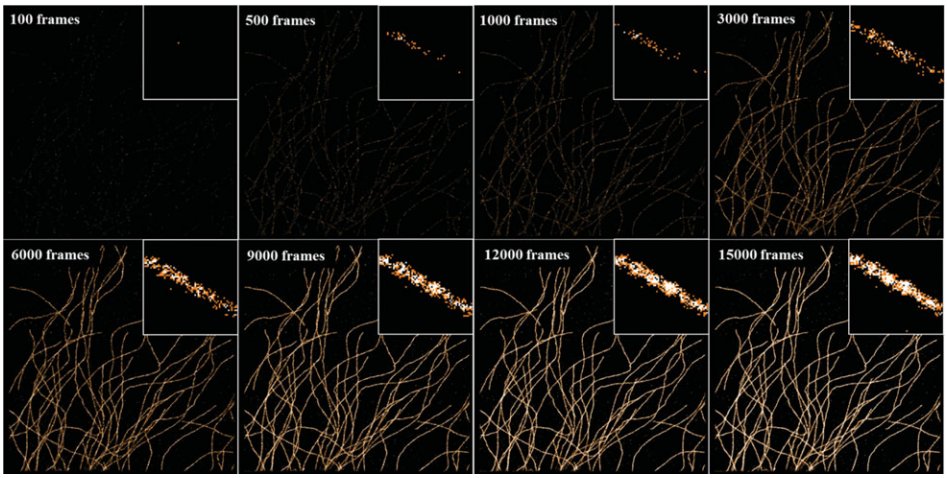

Figure 12.46.10 *(d)*STORM images of microtubules immuno-stained by Alexa Fluor 647 reconstructed by different numbers of imaging frames. The insets show the magnified region.

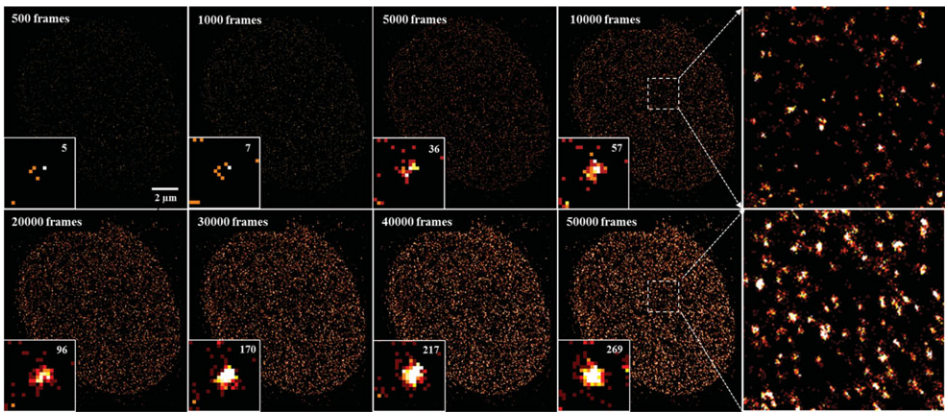

Figure 12.46.11 *(d)*STORM of nucleosomes labeled by histone H2B immuno-stained via Alexa 647 and reconstructed by different numbers of imaging frames. The right two figures show the magnified structure as indicated in the white boxes. Number in the right top of the figure insets is the localization number in the selected area for the same single cluster.

irradiation using low-power, shorter-wavelength lasers (e.g., 405 nm, 488 nm, 532 nm) facilitates the recovery of those "off"-state fluorophores, which can improve the efficiency of image acquisition when the number of "on" molecules becomes too sparse; however, caution should be exercised to avoid significantly overlapping molecules and high background, which can dramatically degrade the localization precision and image resolution.

Multicolor (d)STORM imaging

Multicolor imaging performed by either *(d)*STORM or dye-pair has its advantages and disadvantages, and users should determine the proper method based on the specific application. In the case of *(d)*STORM, sample preparation for multicolor *(d)*STORM is simpler than using dye pairs, which only requires different photo-switching dyes with distinctive emission; most of these fluorophore-conjugated antibodies are commercially available. For image acquisition, only the corresponding lasers for the photo-switching fluorophores are required. However, the chromatic aberration caused by different emission wavelengths is non-negligible at a resolution down to below 100 nm. Therefore, a chromatic correction is required, mostly based on the derived chromatic shift between different color channels from multicolor fluorescent beads (TetraSpeck bead, 0.1 μm diameter, blue/green/orange/dark red fluorescence; Invitrogen, cat. no T7279). However,

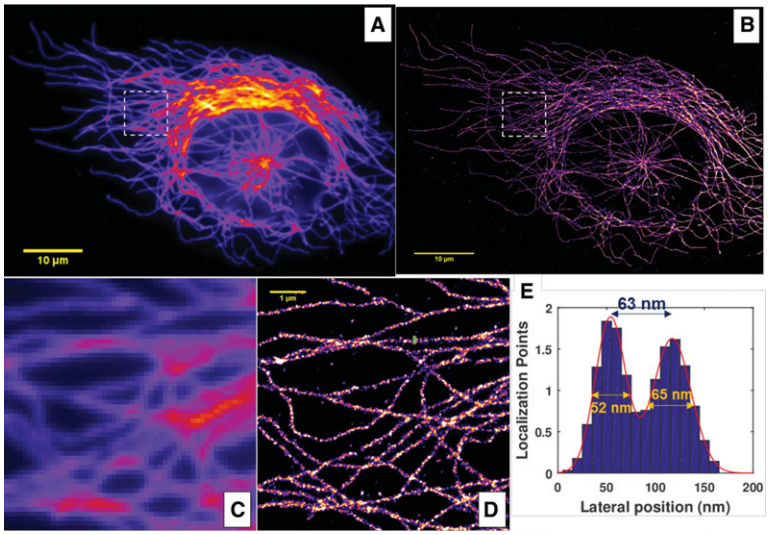

Figure 12.46.12 (**A**-**B**) The conventional wide-field and reconstructed super-resolution image of microtubules from MCF10A cells, immuno-stained with Alexa 647 using *(d)*STORM imaging and reconstructed. (**C**-**D**) The zoomed-in region of the white boxes shown in (A-B), respectively. (**E**) The cross-sectional profile from a marked region in (D), together with the fitted full-width at half-maximum (FWHM). An illumination laser with a wavelength of 642 nm (VFL-P-1000-642-OEM3, MPB Communications) at a power density of 3 kW/cm^2 is used; a total of 40,000 image frames at a speed of 50 Hz (acquisition time of 20 msec) are recorded on an sCMOS camera (pco.edge 4.2, PCO-Tech) with a pixel size of 130 nm on the sample plane. The super-resolution image is reconstructed using the least-squares single-emitter Gaussian fitting method. The extracted molecules are fitted with a least-square single-emitter Gaussian function model. Those candidate molecules that meet the following criteria are rejected: (1) total photon number less than 100; (2) FWHM of PSF 50% larger or smaller than that of the ideal PSF; (3) position with more than 2-pixel distance from the region center; (4) peak intensity versus background intensity less than 0.5. The final super-resolution image was reconstructed by accumulating all molecules that meet the above criteria, with a pixel size of 10 nm followed by a Gaussian smoothing filter ($\sigma = 10$ nm).

due to the heterogeneous aberration in the entire field of view and along the axial direction, such correction has limited accuracy in all three dimensions. In addition, Alexa Fluor 647 is still the best photo-switchable fluorophore for *(d)*STORM imaging, and all other fluorophores have somewhat compromised performance, such as higher background or lower photon counts, which may negatively affect the image resolution.

If the dye-pair method is used, the antibody conjugated to the dye pair usually needs to be synthesized in the laboratory. More importantly, the ratio between the reporter dye and activator dye needs to be well optimized to ensure switching efficiency. Usually at least three activator dyes are conjugated to one reporter dye to minimize the fraction of antibodies labeled with more than one reporter dye, due to the inefficient switching for antibodies labeled with multiple reporter dyes (Bates et al., 2013a). Since the dye-pair mode can use the identical reporter dye for multiple imaging channels, chromatic aberration correction is not required. Another advantage is that we can use the best reporter dye (i.e., Alexa Fluor 647 or its analog Cy5) for multicolor imaging. However, cross-talk is always present if using a dye pair with the same reporter dye. Take the example of two-color STORM imaging with a Cy2-Cy5 pair and a C3-Cy5 pair, respectively. Because the red imaging laser (640 nm) can also excite Cy5 [*(d)*STORM effect], besides the activation lasers for Cy2 and Cy3, there are nonspecific signals from the *(d)*STORM effect of Cy5 in both activation and imaging laser channels, giving a source of color cross-talk, even though this nonspecific cross-talk occurs with a relatively low probability (<5% to 10%). There are some strategies to reduce such nonspecific cross-talk. For example, higher activation laser intensity and lower imaging laser intensity can be used to reduce the nonspecific activation rate. Additionally, only the imaging frame immediately after an activation frame is recognized as a controlled activation event, and the following two frames can be used as nonspecific activation to correct for

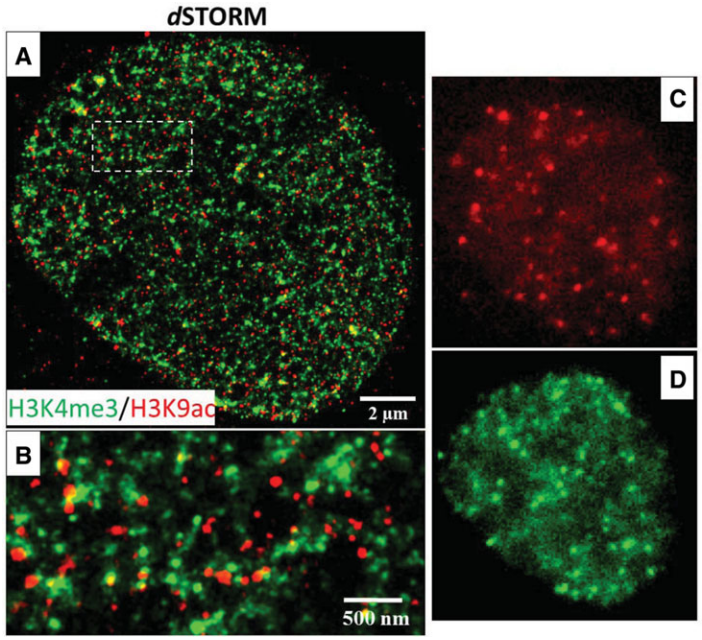

Figure 12.46.13 Two-color super-resolution imaging of methylated (H3K4me3) and acetylated (H3K9Ac) histone proteins by *(d)*STORM. (**A**-**B**) *(d)*STORM images of H3K4me3 and H3K9Ac. H3K4me3 is labeled with Cy3B and H3K9Ac is labeled with Alexa Fluor 647 in the cell nucleus of MCF 10A cells. (**C**-**D**) Representative raw images of Alexa Fluor 647 channel (H3K9Ac) and Cy3B channel (H3K4me3), respectively. Continuous illumination with a 642-nm or 561-nm laser are used in the two-color *(d)*STORM imaging. The two channels are imaged sequentially at an exposure time of 20 msec for 30,000 imaging frames using 642-nm excitation, followed by 30,000 imaging frames using 561-nm excitation. Fluorescent beads (0.1 μm diameter, F8803, excited using 488 nm laser) are used as fiduciary markers on the coverslip to correct for 3-D system drift every 200 frames.

cross-talk (Bates et al., 2007; Dani, Huang, Bergan, Dulac, & Zhuang, 2010).

In addition, an optimized imaging buffer that works well for all fluorescent dyes is needed. In general, imaging buffer containing 2-mercaptoethanol is recommended for Alexa Fluor 647 and Cy3B, and MEA-containing buffer is preferable if ATTO 488 or Alexa Fluor 568 are used. In the case of two-color imaging, for example, if Alexa Fluor 647, ATTO 488, or Alexa Fluor 568 is being used, MEA-containing buffer is recommended. In multicolor STORM imaging with dye pairs, where the blinking fraction also depends on buffers containing different thiols, it has been shown that MEA-containing buffer leads to a lower cross-talk blinking fraction caused by the reporter laser compared to 2-mercapethanol-containing buffer.

Anticipated Results

Single-color (d)STORM imaging

Figure 12.46.12 shows examples of a conventional wide-field image and a reconstructed super-resolution image of microtubules immunostained with Alexa 647 following the sample preparation method described above—single-color *(d)*STORM image acquisition reconstructed using least-squares, single-emitter Gaussian fitting. The *(d)*STORM image (Fig. 12.46.12D) should present a much higher resolution, with clear separation of different microtubule filaments compared to the wide-field image (Fig. 12.46.12C). A cross-sectional profile shown in Fig. 12.46.12E quantifies the size, defined by the full-width at half-maximum, of representative microtubule filaments and their separation distance. The size and the separation distance for two closely spaced microtubules should be approximately 50 to 70 nm. Please note that this refers to randomly selected microtubule filaments, which are neither those of the smallest size nor the hollow structures of a single microtubule. If regions with hollow structures are selected, the expected size should be less than 50 nm.

Two-color (d)STORM imaging

Figure 12.46.13 shows an example of two-color super-resolution images of methylated

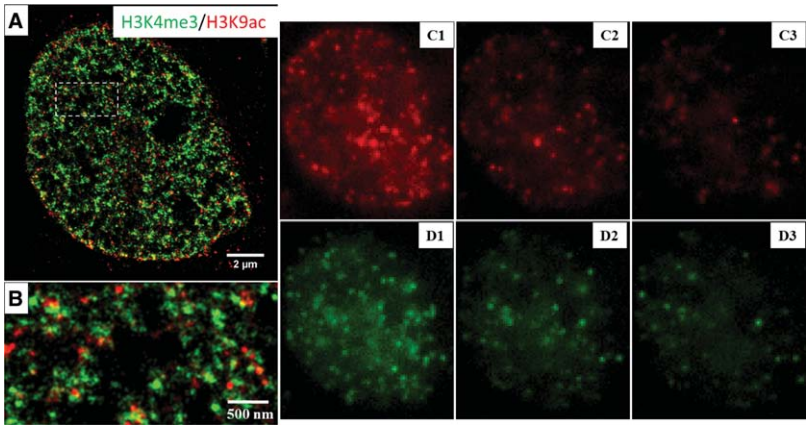

Figure 12.46.14 Two-color super-resolution imaging of methylated (H3K4me3) and acetylated (H3K9Ac) histone proteins by STORM based on dye-pair photo-switchable fluorophores. (**A**-**B**) Reconstructed STORM image. H3K4me3 is labeled with Cy2-Alexa Fluor 647 and H3K9Ac is labeled with Alexa 405-Alexa 647. (**C1-C3**) The representative raw images of the three consecutive frames after activation at 488 nm of the Cy2-Alexa Fluor 647 pair for one cycle. (**D1**-**D3**) The representative three consecutive frames after the activation at 405 nm for an Alexa Fluor 405-Alexa Fluor 647 pair for one cycle. Samples are periodically activated with a sequence of 405-nm and 488-nm laser pulses and then imaged with a 647-nm laser. In each switching cycle, one of the activation lasers is turned on for 1 frame, followed by 3 frames of illumination with the 647-nm imaging laser. The imaging frame immediately after an activation pulse are recognized as a controlled activation event, and a color is assigned accordingly. A total of 40,000 frames include 10,000 activation frames and 30,000 imaging frames for each channel, acquired at an exposure time of 15 msec. A cross-talk subtraction algorithm (described in the protocol) is used to subtract the non-specific activation signal.

and acetylated histone proteins (H3K4me3 and H3K9Ac) in the cell nucleus of MCF 10A cells via two-color *(d)*STORM. Figures 12.46.13A-B show the expected reconstructed two-color images of two histone proteins. Both H3K4me3 and H3K9Ac exhibit nano-size clusters, with a small percentage of co-localization. The representative raw image frames for the Alexa Fluor 647 and Cy3B channels are shown in Figure. 12.46.13C-D, and those bright "dots" are individual fluorescent emitters each fitted with a Gaussian function. It should be noted that for multicolor *(d)*STORM imaging, the longer-wavelength color channel (e.g., 647 nm) should be imaged first to avoid the photobleaching effect caused by the shorter-wavelength laser (e.g., 561 nm laser) due to the overlapping spectra of Cy3B and Alexa 647. If the sequence is reversed, a significant reduction in blinking fluorophores can be seen when the 647-nm color channel is being imaged.

Figure 12.46.14 shows an example of two-color super-resolution images of the same histone proteins (H3K4me3 and H3K9Ac) in the cell nucleus of MCF 10A cells as in Figure 12.46.13 via two-color STORM imaging based on dye-pair photo-switchable fluorophores. The reconstructed two-color STORM image in Figure. 12.46.14A-B shows similar structural features as those in Fig. 12.46.13A-B. The representative three consecutive raw image frames for the Alexa Fluor 405–Alexa Fluor 647 pair are shown in Figure 12.46.14C1-C3). The first frame (Fig. 12.46.14C1) is the image frame right after activation with the 405-nm laser, or controlled activation event; and the subsequent two frames (Fig. 12.46.14C2-C3) are considered nonspecific activation, which accounts for less than 10% of total single fluorescent emitters, and is used to correct for cross-talk between the two color channels.

Time Considerations

Following cell fixation, the immunofluorescence staining step includes a cell permeabilization and blocking step (~1.5 hr), the incubation with primary antibody (overnight), and the incubation with the dye-conjugated secondary antibody (~2 hr). Following immunostaining, image acquisition for each FOV takes about 15 min (if using 50 Hz, 40,000 frames). The speed of image reconstruction following data acquisition depends on the total number of localized molecules,

the localization algorithm, the threshold to identify single fluorescent emitters, and the performance of the computer. For example, if a single-molecule-localization algorithm (integrated Gaussian function, least square optimization method) is used, the time of image reconstruction using ThunderSTORM on a single-core Intel i7-6700 CPU is about 1600 localization events per second; if a multi-emitter Gaussian algorithm is used for high-density localization, time of image reconstruction (based on ThunderSTORM, multi-emitter enabled) on the same computer is about 74 localization events per second.

Acknowledgements

We acknowledge funding support from National Institute of Health, Grant Number R01EB016657 and R01CA185363.

Literature Cited

Bates, M., Jones, S. A., & Zhuang, X. (2013a). Preparation of photoswitchable labeled antibodies for STORM imaging. *Cold Spring Harbor Protocols*, *2013*, 540–541. Available at *http://www.ncbi.nlm.nih.gov/pubmed/23734027*. doi: 10.1101/pdb.prot075168.

Bates, M., Jones, S. A., & Zhuang, X. (2013b). Stochastic optical reconstruction microscopy (STORM): A method for superresolution fluorescence imaging. *Cold Spring Harbor Protocols*, *2013*, 498–520. Available at *http://www.ncbi.nlm.nih.gov/pubmed/23734025*. doi: 10.1101/pdb.top075143.

Bates, M., Huang, B., Dempsey, G. T., & Zhuang, X. (2007). Multicolor super-resolution imaging with photo-switchable fluorescent probes. *Science*, *317*, 1749–1753. Available at *http://www.ncbi.nlm.nih.gov/pmc/articles/PMC2633025/pdf/nihms-88394.pdf*. doi: 10.1126/science.1146598.

Betzig, E., Patterson, G. H., Sougrat, R., Lindwasser, O. W., Olenych, S., Bonifacino, J. S., ... Hess, H. F. (2006). Imaging intracellular fluorescent proteins at nanometer resolution. *Science*, *313*, 1642–1645. doi: 10.1126/science.1127344.

Dani, A., Huang, B., Bergan, J., Dulac, C., & Zhuang, X. 2010. Superresolution imaging of chemical synapses in the brain. *Neuron*, *68*, 843–856. Available at *http://dx.doi.org/10.1016/j.neuron.2010.11.021*. doi: 10.1016/j.neuron.2010.11.021.

Dempsey, G. T., Bates, M., Kowtoniuk, W. E., Liu, D. R., Tsien, R. Y., & Zhuang, X. (2009). Photoswitching mechanism of cyanine dyes. *Journal of the American Chemical Society*, *131*, 18192–18193. doi: 10.1021/ja904588g.

Dempsey, G. T., Vaughan, J. C., Chen, K. H., Bates, M., & Zhuang, X. (2011). Evaluation of fluorophores for optimal performance in localization-based super-resolution imaging. *Nature Methods*, *8*, 1027–1036. Available at http://www.ncbi.nlm.nih.gov/pubmed/22056676. doi: 10.1038/nmeth.1768.

Douglass, K. M., Sieben, C., Archetti, A., Lambert, A., & Manley, S. (2016). Super-resolution imaging of multiple cells by optimized flat-field epi-illumination. *Nature Photonics*, *10*, 705–708. Available at *http://www.nature.com/doifinder/10.1038/nphoton.2016.200*. doi: 10.1038/nphoton.2016.200.

Endesfelder, U. & Heilemann, M. (2015). Direct stochastic optical reconstruction microscopy (dSTORM). In P.J. Verveer (Ed.), *Advanced fluorescence microscopy* (pp. 263–276). New York: Springer.

Galland, R., Grenci, G., Aravind, A., Viasnoff, V., Studer, V., & Sibarita, J.-B. (2015). 3D high- and super-resolution imaging using single-objective SPIM. *Nature Methods*, *12*, 641–644. doi: 10.1038/nmeth.3402.

Gebhardt, J. C. M., Suter, D. M., Roy, R., Zhao, Z. W., Chapman, A. R., Basu, S., ... Xie, X. S. (2013). Single-molecule imaging of transcription factor binding to DNA in live mammalian cells. *Nature Methods*, *10*, 421–426. doi: 10.1038/nmeth.2411.

Gustafsson, M. G. (2000). Surpassing the lateral resolution limit by a factor of two using structured illumination microscopy. *Journal de Microscopie*, *198*, 82–87. Available at *http://www.ncbi.nlm.nih.gov/pubmed/10810003*. doi: 10.1046/j.1365-2818.2000.00710.x.

Heilemann, M., van de Linde, S., Schuttpelz, M., Kasper, R., Seefeldt, B., Mukherjee, A., ... Sauer, M. (2008). Subdiffraction-resolution fluorescence imaging with conventional fluorescent probes. *Angewandte Chemie*, *47*, 6172–6176. Available at *http://www.ncbi.nlm.nih.gov/pubmed/18646237*. doi: 10.1002/anie.200802376.

Hell, S. W. & Wichmann, J. (1994). Breaking the diffraction resolution limit by stimulated-emission—Stimulated-Emission-Depletion Fluorescence Microscopy. *Optics Letters*, *19*, 780–782. doi: http://dx.doi.org/10.1364/OL.19.000780.

Hess, S. T., Girirajan, T. P. K., & Mason, M. D. (2006). Ultra-high resolution imaging by fluorescence photoactivation localization microscopy. *Biophysical Journal*, *91*, 4258–4272. doi: 10.1529/biophysj.106.091116.

Holden, S. J., Uphoff, S., & Kapanidis, A. N. (2011). DAOSTORM: An algorithm for high- density super-resolution microscopy. *Nature Methods*, *8*, 279–280. doi: 10.1038/nmeth0411-279.

Hoogendoorn, E., Crosby, K. C., Leyton-Puig, D., Breedijk, R. M. P., Jalink, K., Gadella, T. W. J., & Postma, M. (2014). The fidelity of stochastic single-molecule super-resolution reconstructions critically depends upon robust background estimation. *Scientific Reports*, *4*, 3854. doi: 10.1038/srep03854.

Huang, F., Hartwich, T. M., Rivera-Molina, F. E., Lin, Y., Duim, W. C., Long, J. J., ... Bewersdorf, J. (2013). Video-rate nanoscopy using sCMOS camera–specific single-molecule localization algorithms. *Nature Methods*, *10*,

653–658. Available at *http://www.ncbi.nlm.nih.gov/pmc/articles/PMC3696415/pdf/nihms475969.pdf*. doi: 10.1038/nmeth.2488.

Huang, F., Schwartz, S. L., Byars, J. M., & Lidke, K. A. (2011). Simultaneous multiple-emitter fitting for single molecule super-resolution imaging. *Biomedical Optics Express*, *2*, 1377–1393. doi: 10.1364/BOE.2.001377.

Lambert, T. J. & Waters, J. C. (2016). Navigating challenges in the application of superresolution microscopy. *The Journal of Cell Biology*, 1–11. doi: 10.1083/jcb.201610011.

Lee, S. H., Baday, M., Tjioe, M., Simonson, P. D., Zhang, R., Cai, E., & Selvin, P. R. (2012). Using fixed fiduciary markers for stage drift correction. *Optics Express*, *20*, 12177–12183. doi: 10.1364/OE.20.012177.

Ma, H., Long, F., Zeng, S., & Huang, Z. L. (2012). Fast and precise algorithm based on maximum radial symmetry for single molecule localization. *Optics Letters*, *37*, 2481–2483. doi: 10.1364/OL.37.002481.

Ma, H., Xu, J., Jin, J., Gao, Y., Lan, L., & Liu, Y. (2015). Fast and precise 3D fluorophore localization based on gradient fitting. *Scientific Reports*, *5*, 14335. doi: 10.1038/srep14335.

Mlodzianoski, M. J., Schreiner, J. M., Callahan, S. P., Smolková, K., Dlasková, A., Šantorová, J., … Je, P. (2011). Sample drift correction in 3D fluorescence photoactivation localization microscopy. *Optics Express*, *19*, 15009. doi: 10.1364/OE.19.015009.

Mortensen, K. I., Churchman, L. S., Spudich, J. A, & Flyvbjerg, H. (2010). Optimized localization analysis for single-molecule tracking and super-resolution microscopy. *Nature Methods*, *7*, 377–381. doi: 10.1038/nmeth.1447.

Mukamel, E. A., Babcock, H., & Zhuang, X. (2012). Statistical deconvolution for super-resolution fluorescence microscopy. *Biophysical Journal*, *102*, 2391–2400. doi: 10.1016/j.bpj.2012.03.070.

Nahidiazar, L., Agronskaia, A. V., Broertjes, J., van den Broek, B., & Jalink, K. (2016). Optimizing imaging conditions for demanding multi-color super-resolution localization microscopy. *PLOS One*, *11*, e0158884. Available at *http://dx.plos.org/10.1371/journal.pone.0158884* [Accessed July 20, 2016]. doi: 10.1371/journal.pone.0158884.

Nieuwenhuizen, R. P. J., Lidke, K. A, Bates, M., Puig, D. L., Grünwald, D., Stallinga, S., & Rieger, B. (2013). Measuring image resolution in optical nanoscopy. *Nature Methods*, *10*, 557–562. doi: 10.1038/nmeth.2448.

Olivier, N., Keller, D., Gönczy, P., & Manley, S. (2013). Resolution doubling in 3D-STORM imaging through improved buffers. *PLoS One*, *8*, e69004. Available at *http://www.ncbi.nlm.nih.gov/pubmed/23874848*. doi: 10.1371/journal.pone.0069004.

Ovesný, M., Křížek, P., Borkovec, J., Švindrych, Z., & Hagen, G. M. (2014). ThunderSTORM: A comprehensive ImageJ plug-in for PALM and STORM data analysis and super-resolution imaging. *Bioinformatics*, *30*, 2389–2390. doi: 10.1093/bioinformatics/btu202.

Parthasarathy, R. (2012). Rapid, accurate particle tracking by calculation of radial symmetry centers. *Nature Methods*, *9*, 724–726. doi: 10.1038/nmeth.2071.

Pertsinidis, A., Zhang, Y., & Chu, S. (2010). Subnanometre single-molecule localization, registration and distance measurements. *Nature*, *466*, 647–651. doi: 10.1038/nature09163.

Quan, T., Li, P., Long, F., Zeng, S., Luo, Q., Hedde, P. N., … Huang, Z.-L. (2010a). Ultra-fast, high-precision image analysis for localization-based super resolution microscopy. *Optics Express*, *18*, 11867–11876. doi: 10.1364/OE.18.011867.

Quan, T., Zeng, S., & Huang, Z.-L. (2010b). Localization capability and limitation of electron-multiplying charge-coupled, scientific complementary metal-oxide semiconductor, and charge-coupled devices for superresolution imaging. *Journal of Biomedical Optics*, *15*, 66005. doi: 10.1117/1.3505017.

Quan, T., Zhu, H., Liu, X., Liu, Y., Ding, J., Zeng, S., & Huang, Z.-L. (2011). High-density localization of active molecules using Structured Sparse Model and Bayesian Information Criterion. *Optics Express*, *19*, 16963. doi: 10.1364/OE.19.016963.

Ricci, M. A., Manzo, C., García-Parajo, M. F., Lakadamyali, M., & Cosma, M. P. (2015). Chromatin fibers are formed by heterogeneous groups of nucleosomes in vivo. *Cell*, *160*, 1145–1158. Available at: *http://www.ncbi.nlm.nih.gov/pubmed/25768910*. doi: 10.1016/j.cell.2015.01.054.

Rust, M. J., Bates, M., & Zhuang, X. W. (2006). Sub-diffraction-limit imaging by stochastic optical reconstruction microscopy (STORM). *Nature Methods*, *3*, 793–795. Available at *http://www.ncbi.nlm.nih.gov/pmc/articles/PMC2700296/pdf/nihms-88406.pdf*. doi: 10.1038/nmeth929.

Sage, D., Kirshner, H., Pengo, T., Stuurman, N., Min, J., Manley, S., & Unser, M. (2015). Quantitative evaluation of software packages for single-molecule localization microscopy. *Nature Methods*, *12*, 1–12. Available at *http://www.ncbi.nlm.nih.gov/pubmed/26076424*. doi: 10.1038/nmeth.3442.

Schneider, C. A., Rasband, W. S., & Eliceiri, K. W. (2012). NIH Image to ImageJ: 25 years of image analysis. *Nature Methods*, *9*, 671–675. Available at *http://www.nature.com/doifinder/10.1038/nmeth.2089* [Accessed January 12, 2017]. doi: 10.1038/nmeth.2089.

Smith, C. S., Joseph, N., Rieger, B., & Lidke, K. A. (2010). Fast, single-molecule localization that achieves theoretically minimum uncertainty. *Nature Methods*, *7*, 373–375. doi: 10.1038/nmeth.1449.

Tokunaga, M., Imamoto, N., & Sakata-Sogawa, K. (2008). Highly inclined thin illumination enables clear single-molecule imaging

in cells. *Nature Methods*, *5*, 159–161. doi: 10.1038/nmeth1171.

van de Linde, S., Loschberger, A., Klein, T., Heidbreder, M., Wolter, S., Heilemann, M., & Sauer, M. (2011). Direct stochastic optical reconstruction microscopy with standard fluorescent probes. *Nature Protocols*, *6*, 991–1009. Available at *http://www.ncbi.nlm.nih.gov/pubmed/21720313*. doi: 10.1038/nprot.2011.336.

Wang, Y., Schnitzbauer, J., Hu, Z., Li, X., Cheng, Y., Huang, Z.-L., & Huang, B. (2014). Localization events-based sample drift correction for localization microscopy with redundant cross-correlation algorithm. *Optics Express*, *22*, 15982–15991. doi: 10.1364/OE.22.015982.

Wolter, S., Löschberger, A., Holm, T., Aufmkolk, S., Dabauvalle, M.-C., van de Linde, S., & Sauer, M. (2012a). rapidSTORM: Accurate, fast open-source software for localization microscopy. *Nature Methods*, *9*, 1040–1041. doi: 10.1038/nmeth.2224.

Wolter, S., Loschberger, A., Holm, T., Aufmkolk, S., Dabauvalle, M. C., van de Linde, S., & Sauer, M. (2012b). rapidSTORM: Accurate, fast open-source software for localization microscopy. *Nature Methods*, *9*, 1040–1041 doi: 10.1038/nmeth.2224.

York, A. G., Ghitani, A., Vaziri, A., Davidson, M. W., & Shroff, H. (2011). Confined activation and subdiffractive localization enables whole-cell PALM with genetically expressed probes. *Nature Methods*, *8*, 327–333 Available at *http://www.ncbi.nlm.nih.gov/pmc/articles/PMC3073501/pdf/nihms266587.pdf*. doi: 10.1038/nmeth.1571.

Zhu, L., Zhang, W., Elnatan, D., & Huang, B. (2012). Faster STORM using compressed sensing. *Nature Methods*, *9*, 721–723. doi: 10.1038/nmeth.1978.